Optimization of the RT-QuIC in prion disease diagnostic

Dissertation

for the award of the degree

“Doctor rerum naturalium (Dr. rer. nat.)”

of the Georg-August University Göttingen

within the doctoral Molecular Medicine

of the Georg-August University School of Science (GAUSS)

Submitted by

Susana Margarida da Silva Correia

from Chaves, Portugal

Göttingen, 2022

Members of Thesis Committee Supervisor

Supervisor

Prof. Dr. Inga Zerr

Department of Neurology

National Reference Center for TSE

Georg-August University

Second member of the thesis committee

Prof. Dr. André Fischer

Department of Psychiatry and Psychotherapy

German Center for Neurodegenerative Diseases (DZNE)

Georg-August University

Third member of the thesis committee

PD Dr. Roberto Goya-Maldonado

Department of Psychiatry and Psychotherapy

Georg-August University

Table of Contents

Abstract

In the present work, we were interested in applying different recombinant prion proteins (rec PrP) as substrates in the real-time quaking-induced conversion (RT-QuIC) assay to improve the diagnostic accuracy in different prion diseases. We were also interested in adapting the RT-QuIC for detecting infectious isoform of prion protein (PrP^{Sc}) in a less invasive biological fluid (tear fluid) samples from prion disease patients. Finally, we intended to study the morphology of fibrils generated during the RT-QuIC by different substrates and the characteristics of the competitive seeding of different rec PrP substrates.

To this aim, hamster-sheep, full-length human (FL Hu), FL Hu with E200K, and fatal familial insomnia (FFI) mutations were produced and purified through fast protein liquid chromatography (FPLC). Subsequently, different rec PrP substrates were tested in the RT-QuIC using CSF and tear fluid from patients with prion and non-prion disease controls. In the CSF RT-QuIC, we observed an increase of the sensitivity in prion diseases 95% sCJD patients (with different codon PRNP 129 MV geno- and subtypes), 100 % in E200K, and 88 % in FFI) when using FL Hu E200K substrate compared to hamster-sheep (84.6 % in sCJD, 88 % in E200K, and 23 % in FFI) and FL Hu (76 % in sCJD, 88 % in E200K, and 36 % in FFI) substrates (retrospective study). We also observed a reduced lag phase duration and higher area under the curve (AUC) values when using FL Hu E200K substrate (compared to the other substrate) in different prion diseases.

Consequently, a reduction of the duration of the assay to 60 h (instead of 80 h) can be considered. Another prospective study comparing the agreement between the rec Hu E200K substrate with the hamster-sheep (in routine use) revealed a substantial agreement between both substrates.

Transmission electron microscope studies indicated different subtle morphologies of PrP-fibrils generated during the RT-QuIC with different rec substrates. A mixture of different rec PrP substrates (e.g., Hu E200K substrate with hamster-sheep) provoked a mean signal response in the RT-QuIC, which indicates that two rec PrP substrates with different *PRNP* sequences do not inhibit each other; they were able to convert and aggregate independently from each other.

In tear fluid samples from prion disease patients, we used the higher sensitive FL Hu E200K substrate in the RT-QuIC. Here, we observed a sensitivity of 75 %, while the specificity remained at 100 %.

Our study demonstrated that using the FL Hu E200K substrate in the CSF RT-QuIC improved the sensitivity of the assay, in particular for FFI diagnosis, and it enables the detection of PrP^{Sc} in less-invasive tear fluid samples, which may be quite useful not only for diagnostic but also for follow-up studies (e.g., after therapeutic intervention).

List of figures

List of tables

List of abbreviations

aa	Amino acid
ADC	Apparent diffusion coefficient maps
AUC	Area under curve
ATP	Adenosine triphosphate
bp	Base pair
BSE	Bovine spongiform encephalopathy
^{o}C	Celsius
CDC	Centers for Disease Control and Prevention
CP	choroid plexuses
CSF	Cerebrospinal fluid
CJD	Creutzfeldt-Jakob disease
dH_20	Distilled water
ddH_2O	Double distilled water
D	Aspartate amino acid
DNA	Deoxyribonucleic acid
D178N	Carried a CJD-specific mutation at codon 178 of the PrP gene
DWI	Diffusion weighted images
E	Glutamate

OM	Olfactory mucosa
OPR	Octapeptide repeats
EDTA	Ethylenediaminotetraedric acid
ECL	Enhanced chemiluminescence
EEG	Electroencephalogram
ELISA	Enzyme-Linked Immunosorbent Assay
ER	Endoplasmic reticulum
E200K	Carried a CJD-specific mutation at codon 200 of the PrP gene
fCJD	Familiar Creutzfeldt-Jakob disease
FFI	Fatal familial insomnia
FPLC	Fast protein liquid chromatography
FL Hu	Full-length Human
FLAIR	Fluid attenuated inversion recovery images
gCJD	Genetic CJD
GPI	Glycosyl-phosphatidylinositol
GSS	Gerstmann–Sträussler–Scheinker disease
h	Hour
iCJD	Iatrogenic Creutzfeldt-Jakob disease
K	Lysine

kDa	Kilodalton
L	Liter
M	Mol
M	Methionine
mM	millimolar
MRI	Magnetic resonance imaging
mg	Milligram
min	Minutes
ml	Milliliter
N	Asparagine amino acid
NaCL	Sodium chloride
nm	Nanomiter
NMDA	N-methyl-D-aspartate receptors
p	Probability value
PBS	Phosphate buffered saline
PET	Positron emission tomography
PNGase	Enzyme peptide N glycosidase F
PVDF	Polyvinylidene fluoride
PrP	Prion protein

PrP^{C}	Cellular prion protein
PrP^{Sc}	Infectious isoform of prion protein
PrP^{Res}	Prion protein resistant to proteases
PRNP	Prion protein gene
PSWC	Sharp wave complexes
rec PrP	Recombinant PrP
r.f.u	Relative fluorescence intensity
RT	Room temperature
rpm	Revolutions per minute
RT-QuIC	Real-time quaking-induced conversion
s	second
sCJD	Sporadic Creutzfeldt-Jakob disease
SDS-PAGE	Sodium Dodecyl Sulphate Polyacrylamide Gel Electrophoresis
SPECT	Single-photon emission tomography
SOC	Super optimal broth with catabolite repression
STI1	Stress inducible protein 1
TBS	Tris buffered saline
TBST	TBS with 0.1% Tween
TE	Tris EDTA buffer88

TEM	Transmission electron microscopy
Th-T	Thioflavin T
Tris	tris(hydroxymethyl)aminomethane
TSE	Transmissible spongiform encephalopathies
UV	Ultra violet
V	Valine
vCJD	Variant Creutzfeldt-Jakob disease
WHO	World Health Organization
WB	Western blot
µg	Microgram
µl	Microliter
µm	Micro meter
x g	Number of times the gravitational force
%	Percentage

I. Introduction

1. Cellular prion protein (PrP^C)

The cellular prion protein (PrP^C) is a glycosyl-phosphatidylinositol (GPI)-anchored glycoprotein, highly expressed in the brain and spinal cord region [1]. Although the physiological function of PrP^C is still unclear, some putative functions such as synaptic transmission and plasticity [2,3], memory formation [4,5], stabilization of sleep and circadian rhythm [6], neuronal excitability [3,7–10], calcium homeostasis [9–11], glutamate receptor function [12–14], neurite outgrowth [11,15,16], toxicity elicited by oligomeric species [17], neuroprotection [18–20]; copper, zinc, iron, and lactate metabolism [21–24], peripheral myelin maintenance [25,26], receptor for amyloid beta in Alzheimer's disease and possibly for other amyloids are some functions attributed to the physiological PrP^C [17,27,28]. By unknown mechanisms, the PrP^C undergoes a structure conformal change that could lead to severe neurodegenerative diseases [29].

The PrP^C unglycosylated or glycosylated (mono and di-) forms (Figure 1) are synthesized in the endoplasmic reticulum (ER), following transportation to the Golgi apparatus for further modifications before being transferred to plasma membrane in its mature form [30].

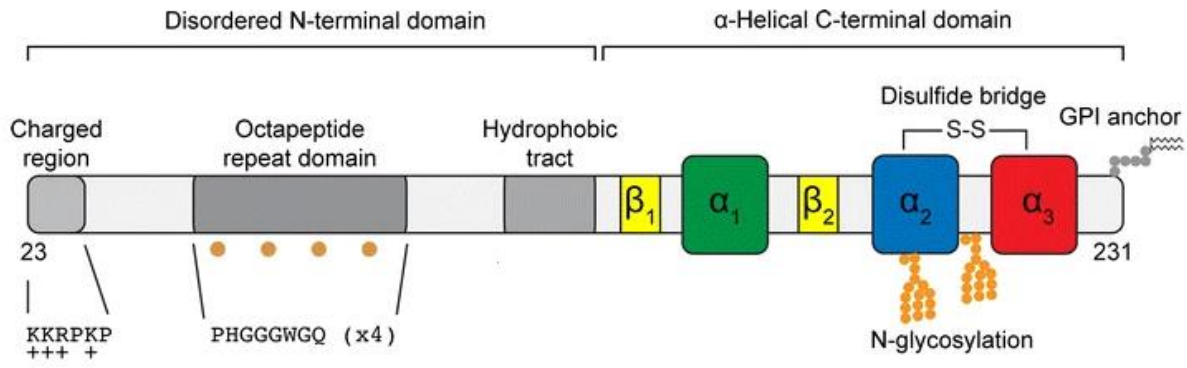

Figure 1. Structure of PrP^C, including glycosylation sites and disulfide bridge.

The PrP^C comprises two distinct structural domains: an N-terminal disordered domain and a C-terminal α-helical domain. The N-terminal domain includes a positive charge region essential for the endocytosis of the PrP^C. The Octapeptide region comprises four octapeptide repeats that allow the binding of PrP^C to ions as a Cu^{2+}/Zn^{2+} and a hydrophobic tract. The C-terminal domain includes three α-helices and two short β-

strands. This domain is subject to posttranslational modifications, such as the addition of one or two N-glycans in the α-helical domain and the GPI anchor at the C-terminus that allows the attachment of the PrP^C to the outer surface of the plasma membrane. Figure taken from Watts *et al*. (2018) [31].

1.1 Structure of cellular and infectious isoform of prion protein

The non-pathogenic form of PrP^C comprises α-helix (~ 40 % of protein), separated by a loop/turn region and two small regions of β-sheet structures (~ 3 % of protein). Physiological PrP^C is sensitive to proteolysis. Although, under unknown mechanisms, PrP^C undergoes structural changes leading to an increase of beta-sheet structures in 3% to 40%, becoming misfolded and resistant to protease digestion, known as the scrapie isoform of the prion protein (PrP^{Sc}) [32,33]. The conversion of PrP^C into PrP^{Sc} can occur by infection when external PrP^{Sc} interacts with the physiologic PrP^C or by a poorly understood pathway where the PrP^C changes its conformation into PrP^{Sc} (Figure 2). Ultimately, this conversion leads to cell apoptosis due to the accumulation of PrP^{Sc} [34–36].

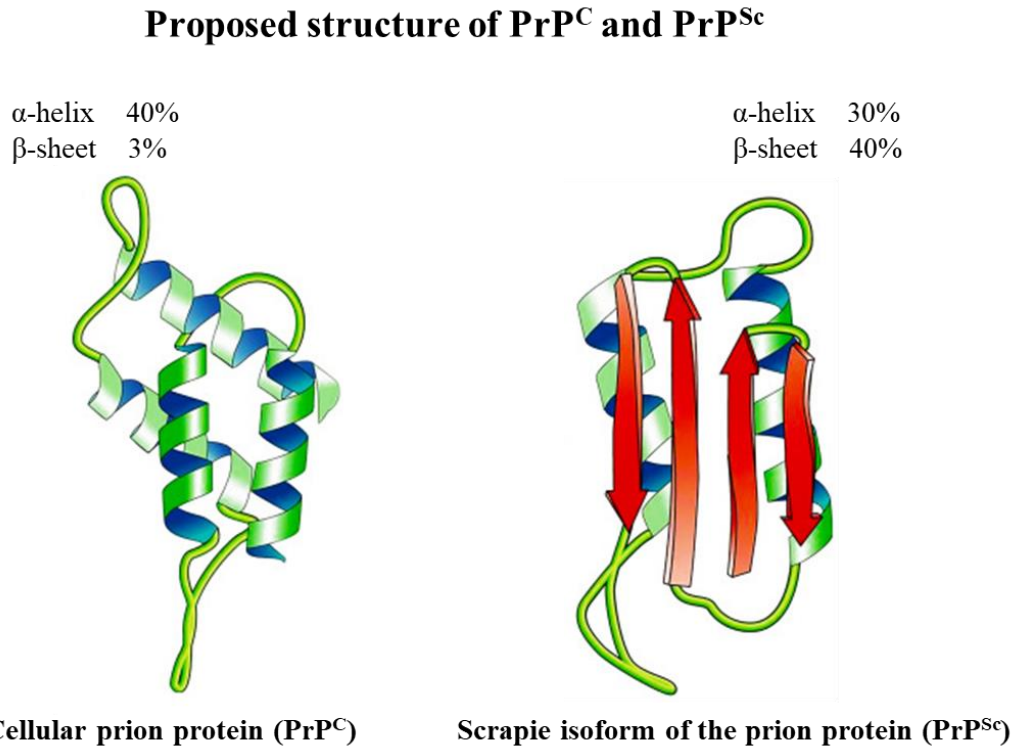

Figure 2. Structure of PrP^C and PrP^{Sc}.

Cellular prion protein and Scrapie isoform of the prion protein structures. Figure taken from Burrel *et al*. (2016) [37].

1.2 Prion protein resistant to proteases (PrP^{Sc}) and prion diseases

The intracellularly and extracellularly accumulation of PrP^{Sc} is a feature of neurodegenerative diseases called transmissible spongiform encephalopathies (TSE), also known as prion diseases. The PrP^{Sc} aggregates lead to neurological dysfunctions and cell death. In the brain, neurons start to die; with the advancement of the disease, neuronal death is higher, and the brain acquires a sponge form. TSE is a group of neurodegenerative diseases that inevitably leads to death in humans and other mammals [38]. In mammals, the TSE occurs as scrapie disease (sheep), transmissible mink encephalopathy (mink), chronic wasting disease (deer), bovine spongiform encephalopathy (cattle), and feline spongiform encephalopathy (cats). The most common prion disease in humans is sporadic Creutzfeldt-Jakob disease (sCJD) (Table 1) [34,35].

Table 1. Transmissible spongiform encephalopathies (TSE) in humans and animals [39–41].

Disease	Animal species	Etiology
Scrapie	Sheep	Infection
Transmissible mink encephalopathy	Mink	Infection
Chronic wasting disease	Deer	Infection
Bovine spongiform encephalopathy	Cows and Cattle	Infection
Feline spongiform encephalopathy	Cats	Infection
Creutzfeldt-Jakob disease **Iatrogenic** **Sporadic** **Familiar** **New variant**	Humans	 Infection Unknown Mutation in PrP gene Infection from bovine prion?
Fatal familiar insomnia	Humans	Mutation in PrP gene
Sporadic familiar insomnia	Humans	Unknown
Gerstmann–Sträussler–Scheinker disease	Humans	Mutation in PrP gene

2. Creutzfeldt-Jakob disease (CJD)

Creutzfeldt–Jakob disease (CJD), also known as prion disease, is a group of rare and invariably fatal neurodegenerative diseases in humans that affects approximately one person per million per year [42]. However, due to the complex diagnosis, this number may be higher.

Iatrogenic, sporadic, familiar, and new variant CJD are the four different types of CJD grouped according to their etiology. Sporadic CJD (sCJD) is the most common form of CJD, and the conversion of PrP^{C} into PrP^{Sc} occurs for an unknown reason. The course

of the disease is shorter than in other forms and typically affects adults between the ages of 60 and 65 [43,44]. Familiar CJD (fCJD) is the second most common type of CJD, and the cause of the conversion of PrP^{C} into PrP^{Sc} is associated with different mutations in the prion protein gene (*PRNP*). The age of onset in the fCJD can be younger than 60 to 65 years old, and the course of the disease is generally longer than in sCJD [45].

The iatrogenic type of CJD (iCJD) accounts for a tiny percentage of cases, and the conversion of PrP^{C} into PrP^{Sc} is associated with contamination of PrP^{Sc} through a medical procedure such as brain surgery, a corneal transplant or dura mater grafts. In the new variant CJD (vCJD), commonly known as mad cow disease, the infection source is associated with consuming beef contaminated with bovine spongiform encephalopathy (BSE). The age of onset is typically younger, and the disease duration is longer than in the sCJD [46].

2.1 Sporadic Creutzfeldt-Jakob disease (sCJD)

The sporadic Creutzfeldt-Jakob disease (sCJD) is the most common form of prion disease in human; approximately 85 % to 95 % of human CJD cases are sporadic [47,48]. The cause of sCJD is unknown, and the disease is not associated with any mutation in the *PRNP* gene. Although, studies have been reporting that people with a family history of CJD, a medical history of psychosis, a history of multiple surgical procedures, and residence for more than ten years on a farm have a significant risk of developing sCJD [49].

The sCJD is the prion disease with the highest degree of phenotypic heterogeneity associated with the polymorphisms of codon 129 in the *PRNP* and with the size of the protease-resistant core of the PrP^{Sc}, ~21 KDa (type 1) and ~19KDa (type 2). In codon 129 of the *PRNP*, an amino acid methionine (M) or valine (V) is present for each allele. Depending on the genotype of the codon 129, the patients with CJD can have the genotype MM, MV, or VV in the protease-resistant core. The different genotypes and sizes of protease-resistant core (type 1 and 2) lead to a different phenotype of prion disease (Figure 3) [50]. Accordingly, with the genotype and protease-resistant core, sCJD is subdivided into six subtypes, sCJD MM1, sCJD MM2, sCJD MV1, sCJD MV2, sCJD VV1, and sCJD VV2. Two types of sCJD, sCJD cognitive and sCJD ataxic, grouped the six subtypes according to their clinical and histopathological features [51,52].

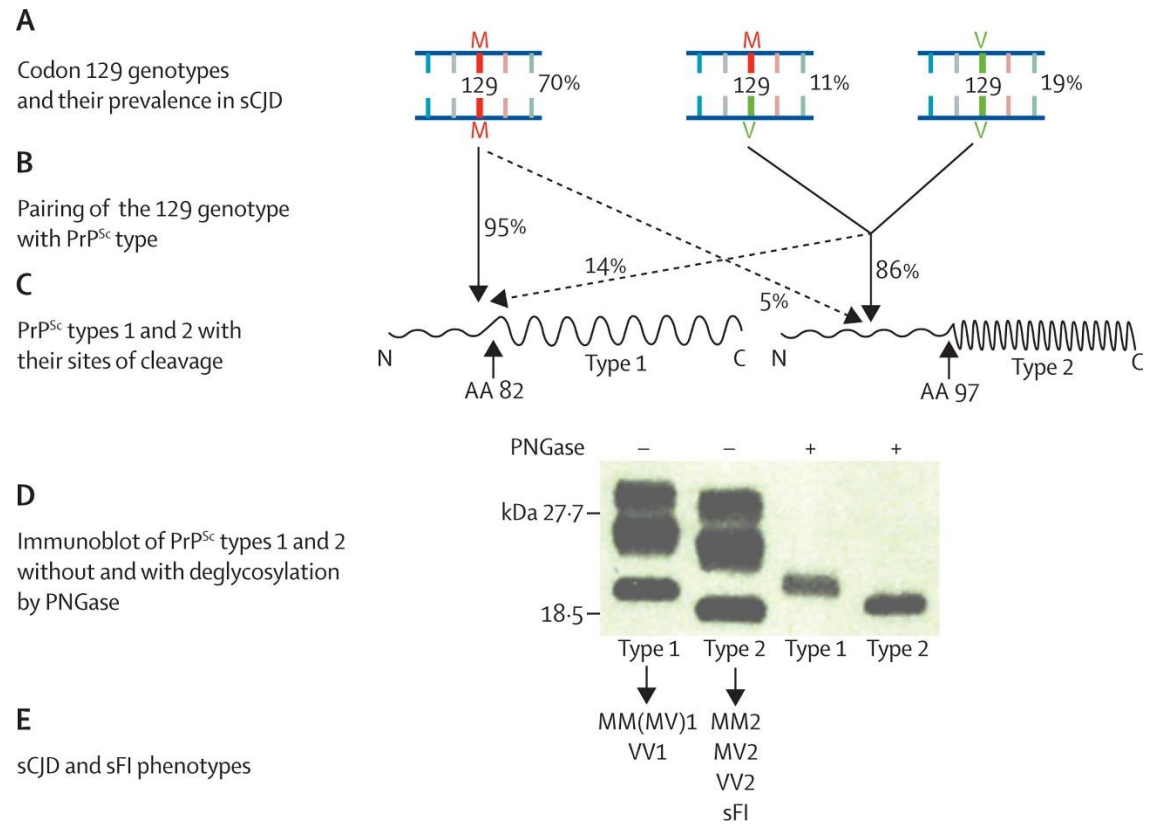

Figure 3. Correlation between the polymorphisms at codon 129 of *PRNP* gene and different types of PrP^{Sc} protease-resistant core.

(A) The diagram represents different genotypes in the *PRNP* gene and their prevalence in sCJD patients. (B) 95 % of the sCJD cases are associated with MM genotype and PrP^{Sc} type 1, whereas 86 % of cases are associated with MV and VV genotype and PrP^{Sc} type 2. (C) The conformation between PrP^{Sc} types 1 and 2 is related to different protease-sensitive cleavage sites. In PrP^{Sc} types 1, the protein is digested down to amino acid (aa) 82, while in PrP^{Sc} types 2, the protein is digested down to aa 97. (D) Electrophoretic mobilities of the protease-resistant fragments of the PrP^{Sc} types 1 and 2. The molecular weight of the protease-resistant fragments of the PrP^{Sc} type 2 is smaller than type 1 and can be easily distinguished in the immunoblot, especially after cleavage of the sugars by the enzyme peptide N glycosidase F (PNGase). (E) The different genotypes and PrP^{Sc} types are determinants for the phenotypes of sCJD commonly identified with letters and numbers to indicate the associated genotype and PrP^{Sc} type. Figure taken from Puoti *et al*. (2012) [40].

2.1.1 sCJD classification according to the clinical characteristics

Cognitive decline and ataxia are the two groups of sCJD divided according to the clinical characteristics of the disease (phenotype). In the cognitive group, the majority of

the patients present cognitive decline (70-100%), and just a tiny percentage of the patients present ataxia (13-39 %), while in the ataxia group, the majority of the patients present ataxia (81-98 %) and with the advanced stage of the disease the percentage of patients presenting increase to 100 % [52]. sCJD MM1 or MV1 (the classic forms), sCJD MM2, and sCDJ VV1 are the three subtypes of the cognitive group, and sCDJ VV2 and sCDJ MV2 are the subtypes of the ataxia group divided according to the phenotype of the disease.

2.1.1.1 Symptomatic cognitive group

2.1.1.1.1 Subtype sCJD MM1 and sCJD MV1

sCJD MM1 and MV1, also known as classic CJD, are a subtype of the symptomatic cognitive group and account for approximately 60 to 70 % of sCJD cases and are observed in individuals with genotype MM or MV at codon 129 of the PrP gene carring PrP^{Sc} type. However, approximately 95 % of individuals in this subgroup belong to the MM1 genotype, while the individuals with genotype MV1 are rare [53,54]. The MM1 and MV1 genotypes are clinical and histopathologically indistinguishable. The difference between both is the 129 genotype. Therefore, the MM1 and MV1 belong to the same subtype [52,55]. The mean age at the onset of the disease is around 66 years old, and this subtype has a short duration of illness. When patients have severe signs of the disease in a few weeks, enter a vegetative state and die, the mean duration of the disease is four months after onset [50]. Rapidly progressive cognitive decline, such as memory loss and confusion/disorientation, occasionally accompanied by cortical visual disturbances, are the characteristic phenotype of this subtype. In the initial stage, the cognitive decline appears in approximately 70 % of patients and, in a short time, rises to 93 %. The patients also present ataxia in this subtype, about 53 % percent in the advanced stage. Approximately 97 % of patients have a spontaneous or induced myoclonus and mild psychiatric symptoms such as depression, anxiety, and psychosis [36,40,56]. The patients with sCJD MM1 subtype exhibit elevated levels of 14-3-3 protein and Tau in cerebrospinal fluid (CSF), and they are associated with periodic sharp wave complexes (PSWC) on electroencephalogram (EEG). These three characteristics are typical in sCJD MM1 [40,56,57].

2.1.1.1.2 Subtype sCJD MM2

This rare subtype accounts for 2 to 10% of sCJD cases. It is observed in individuals with genotype MM2 at codon 129 of the PrP gene and carries PrP^{Sc} type 2. The average age onset of this subgroup is around 66 years, and the disease duration is about 14 months after the onset [50,58]. Cognitive decline in all patients and amnestic aphasia in an initial stage in about 32 % of patients are the characteristic phenotype of this subtype. During the illness, amnestic aphasia increases to 72 % of patients, and the patients occasionally feature pyramidal signs, apraxia, Parkinsonism, and myoclonus [36,56,59]. About 24 to 44 % of the patients present PSWC on EEG in the intermediate and advanced stages of the disease. The 14-3-3 and Tau CSF tests are positive in approximately 50 % of all cases of sCJD MM2. However, magnetic resonance imaging (MRI) showed abnormal imaging in most (93 %) of patients [40].

2.1.1.1.3 Subtype sCJD VV1

This rare subtype accounts for approximately 1 to 4 % of sCJD cases. It is the most uncommon prion disease. This subtype is observed in individuals with genotype VV1 at codon 129 of the PrP gene and carry PrP^{Sc} type 1. The mean age onset of this subgroup is around 43 years old, and it has a long duration of illness, about 19 months after onset. It is difficult to distinguish the patients from this subgroup from the sCJD MM2 patients in the initial stage. Both subtypes have a cognitive decline, and patients can remain mono-symptomatic for several months [60]. However, in patients with the sCJD VV1 subtype, the cognitive decline is slower than in patients with sCJD MM2 and is occasionally associated with personality changes. All patients present cognitive decline throughout the illness and occasionally feature psychiatric symptoms, pyramidal signs, Parkinsonism, and myoclonus [50,60]. The patients with sCJD VV1 subtype have a presence of 14-3-3 and Tau protein in CSF, and the EEG shows non-specific slowing but not PSW complexes. Moreover, the patients with sCJD VV1 exhibit abnormal MRI patterns [40,56,57].

2.1.1.2 Symptomatic sCJD ataxia group

2.1.1.2.1 Subtype sCJD VV2

This subtype accounts for approximately 16 % of sCJD cases and is observed in individuals with genotype VV at codon 129 of the PrP gene and carring PrP^{Sc} type 2. The mean age onset of the disease is around 64 years old, and the duration of illness is about six months after onset [50,61]. The characteristic phenotype of this subtype is the presence of ataxia in almost all patients in the initial state of disease is a characteristic of this subgroup. Throughout the illness, all patients have cognitive decline and ataxia. In this subtype, it is also characteristic of myoclonus (approximately 66 % of patients) and pyramidal signs (50 % of patients) [36,40,56]. The patients with sCJD VV2 subtype have a presence of 14-3-3 and Tau protein in the CSF. The MRI is abnormal in approximately 60 % of the patients [40].

2.1.1.2.2 Subtype sCJD MV2

This subtype accounts for approximately 9 % of sCJD cases and is observed in individuals with genotype MV at codon 129 of the PrP gene and carring PrP^{Sc} Type 2. The mean age onset of the disease is about 64 years old, and the duration of illness is about 17 months after onset [50,62]. Ataxia in almost all patients and cognitive decline in the initial state of disease is a typical characteristic phenotype of this subtype. Throughout the illness, all patients have cognitive decline and ataxia. The patients occasionally feature Parkinsonism, myoclonus, and psychiatric signs [36,40,56]. The patients with sCJD MV2 subtype have a presence of 14-3-3 and Tau protein in the CSF. The MRI is also abnormal in all patients [40].

3. Diagnostic of sCJD

Effective therapeutics for CJD patients are currently unavailable, and accurate *pre-mortem* diagnosis can be challenging. According to diagnostic criteria released by the Centers for Disease Control and Prevention (CDC) [63], only standard neuropathological techniques such as immunohistochemistry and western blot that confirmed the presence of PrP^{Sc} in brain tissue, usually performed at postmortem examination, are valid for a definitive diagnosis of CJD. However, patients can be diagnosed as a probable or possible

case of sCJD in antemortem diagnosis when they fulfill the clinical diagnostic criteria for sCJD (Figure 4), and other neurodegenerative diseases have been ruled out. A combination of characteristic neuropsychiatric symptoms, EEG, MRI, CSF 14-3-3 protein, and RT-QuIC is the base for the clinical diagnostic of CJD at the *pre-mortem*. Biomarkers such as high CSF total Tau may contribute to a better accurate *pre-mortem* diagnostic. Although, discordant results of studies have led to controversies about the clinical value of some established surrogate biomarkers [64].

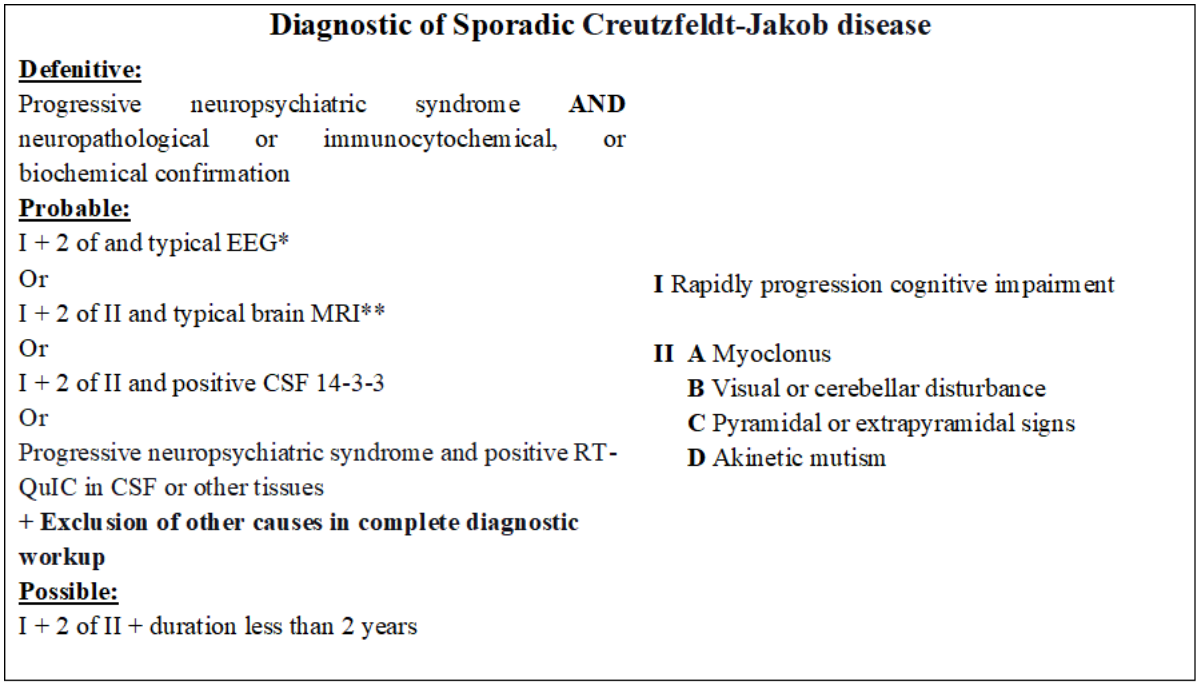

Figure 4. Criteria for the clinical diagnosis of sporadic Creutzfeldt-Jakob disease.

Clinical diagnostic criteria for diagnosis of definitive, probable, and possible sCJD.

* Periodic sharp wave complexes (PSWC) on EEG

** High signal either on DWI or FLAIR MRI sequence in at least two cortical regions (temporal, parietal, occipital) or at the caudate nucleus and putamen. Figure from Herman *et al*. (2022) [65].

3.1 Electroencephalogram (EEG)

Periodic sharp wave complexes (PSWC) on EEG represent the most typical finding during the illness course of the patients with sCJD with a sensitivity of 64 % and specificity of 91 % [66]. PSWC is not just an essential indicator of sCJD but also has excellent interobserver reliability between different EEGs, which allows a reliable and valid EEG evaluation [67]. The PSWC is diagnosed in the EEG recordings if the record contains strictly periodic cerebral potentials, the majority with a duration between 100 and 600 milliseconds and an inter-complex interval between 500 and 2,000 milliseconds based on the EEG studies on periodic complexes in pathologically confirmed CJD [68–71]. Semiperiodic complexes, defined as complexes without at least five repetitive intervals with a duration difference of fewer than 500 milliseconds, were not accepted as PSWC. Although generalized and lateralized complexes are considered PSWC [72]. Depending on the sCJD subtype, the PSWC could be detected on the EEG in the very early stages of the disease (1–4 months after onset) in the case of the MM1/classic sCJD group (Figure 5) or only in the later stages of the disease (27–58 months after onset), MM2C-sCJD group (Figure 6) [73].

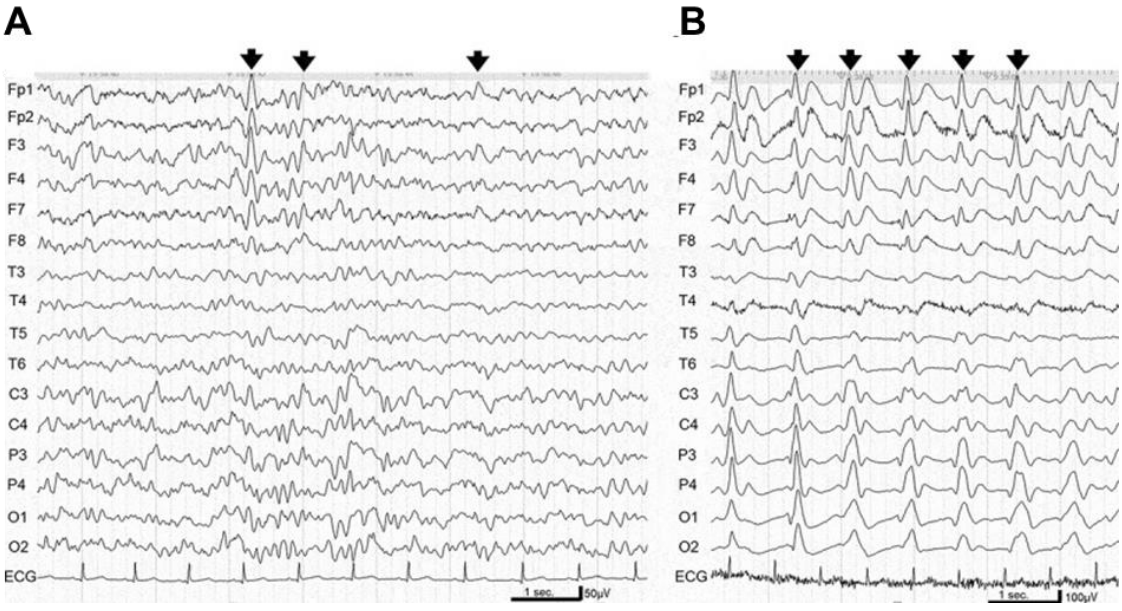

Figure 5. Electroencephalogram (EEG) in sCJD MM1 subtype.

(A) EEG readings a month after the disease onset (early stage) showed background activity and triphasic waves or lateralized frontal dominant sharp (black arrows). (B) EEG readings after 4 months after disease

onset (later stage) showed poorly organized background activity and periodic sharp wave complexes (black arrows). Figure taken from Matsubayashi *et al*. (2020) [73].

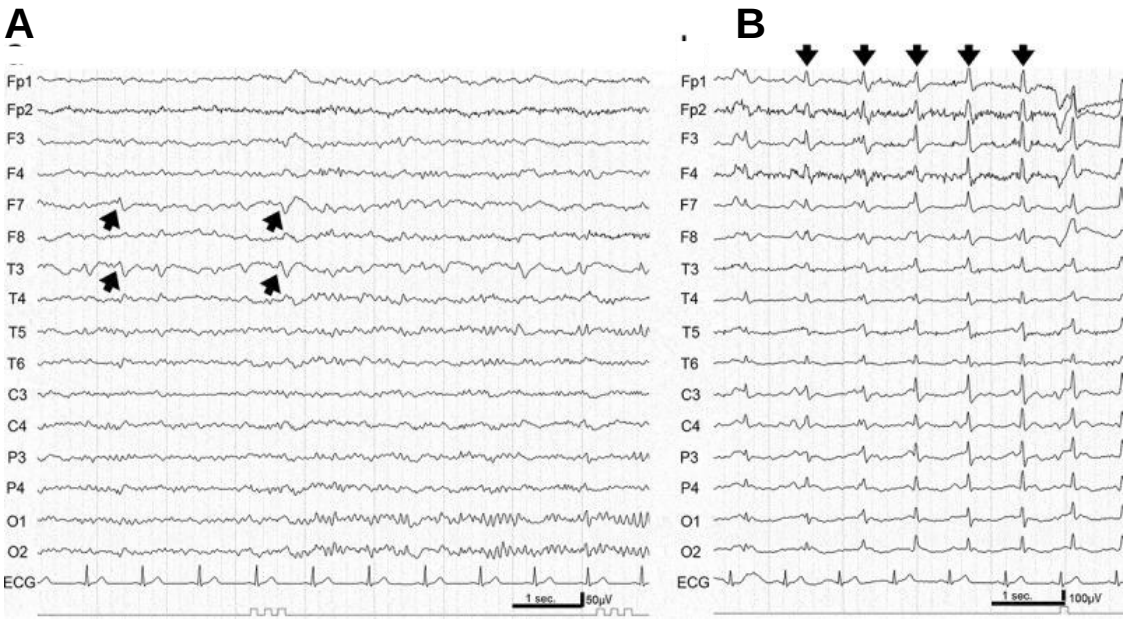

Figure 6. Electroencephalogram (EEG) in MM2C sCJD.

(A) EEG readings 10 months after the disease onset (early stage) showed background activity and focal discharges at F7 and T3 (black arrows). (B) EEG readings 58 months after disease onset (late stage) showed low amplitude background activity and periodic sharp wave complexes (black arrows). Figure taken from Matsubayashi *et al*. (2020) [73].

3.2 Magnetic resonance imaging (MRI)

In recent years magnetic resonance imaging (MRI) has become increasingly important in identifying differential diagnoses, such as ischemia, encephalitis, and neoplasia. Furthermore, combining different MRI pulse sequences has proved to be a valid additional parameter for "probable" sCJD diagnosis when discarded another possible neurodegenerative disease in the patient's diagnosis. Diffusion-weighted images (DWI) and fluid-attenuated inversion recovery (FLAIR) sequences in the MRI have shown to be the best of the four MRI techniques (T2-weighted images, FLAIR images, DWI, and Proton-Density-Weighted images) to show characteristics of pathologic changes in sCJD patients (pathologic changes detected in 76,6 % and 47,3 % of cases, respectively) (Figure 7) [74]. Therefore, DWI and FLAIR MRI sequences were proposed in 2009 to be added to

the World Health Organization (WHO) sCJD diagnosis criteria. According to these criteria, an MRI brain scan is positive for sCJD diagnosis when at least in two cortical regions (temporal, parietal, occipital) or at the caudate nucleus and putamen shows a high signal either on DWI or FLAIR sequence [75]. The combination of those MRI sequences showed to be highly specific (96 %) and have a higher sensitivity (80 %) than CSF biomarkers as 14-3-3 (50 %), T-tau (68 %), and EEG (44 %) [76,77]. Another widely used protocol recommends using DWI and apparent diffusion coefficient (ADC) maps. According to this protocol, if at least one of the eight brain regions (cortical regions (frontal and parietal, including the precuneus, temporal and occipital lobes) shows hyper-intensity in DWI associated with low diffusivity on ADC maps, the MRI scan is considered positive for sCJD. This protocol showed higher sensitivity and interobserver reliability. The sensitivity of MRI from four different neuroradiologists was between 90-95 %, compared with that obtained by using the current criteria (69-76 %) (combination of DWI and FLAIR sequences), while specificity remained unchanged, 90 to 100 % [78].

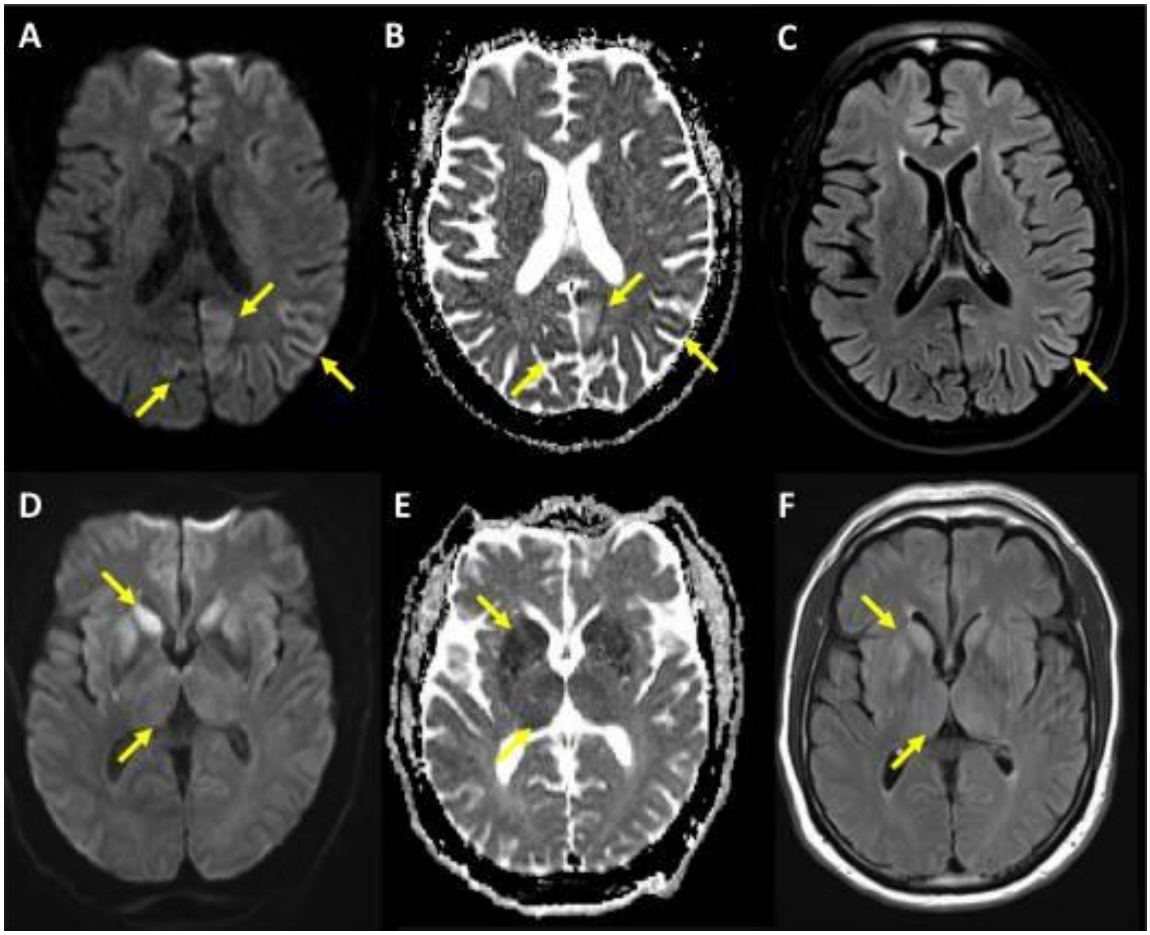

Figure 7. Pathologic changes characteristics on MRI sCJD patients.

(A-C) Occipital and parietal lobes from an MM1 sCJD patient showed restricted diffusion, more pronounced in the left hemisphere (yellow arrows). Hyperintensities were more pronounced on diffusion-weighted images **(A)** than on fluid-attenuated inversion recovery images (C). (B) Associated hypointensities on apparent diffusion coefficient maps (ADC). (D-F) The caudate nucleus, putamen, and thalamus from a VV2 sCJD patient showed restricted diffusion in both hemispheres (yellow arrows) on diffusion-weighted images (D) and fluid-attenuated inversion recovery images (F). (E) Associated hypointensities on apparent diffusion coefficient maps (ADC). Figure taken from Hermann *et al.* (2022) [65].

3.3 Real-Time Quaking-Induced conversion (RT-QuIC)

The real-time quaking-induced conversion (RT-QuIC) assay is a significant breakthrough in the *pre-mortem* diagnosis of sCJD, with high reproducibility between different laboratories and the highest sensitivity (80-89 %) and specificity (99-100 %) for sCJD compared to other current methods [79–83]. RT-QuIC assay mimics the seeded

conversion process of PrP^{C} *in vitro*, amplifying minuscule amounts of a PrP^{Sc} derived from brain, CSF, olfactory mucosa (OM) brushings, or other tissues to an aggregated form of prion protein resistant to proteases (PrP^{Res}) [84,85]. During the RT-QuIC, patients' samples are mixed with the recombinant PrP (rec PrP) and thioflavin T (Th-T) and subjected to incubation and vigorous shaking cycles. In the RT-QuIC incubation step, the rec PrP converts into PrP^{Res} when it enters contact with a patient sample containing PrP^{Sc}. After incubation, the RT-QuIC starts the shaking step program, leading to the fragmentation of the PrP^{Res} aggregates into smaller conversion-competent seeds. After incubation, the RT-QuIC change to the shaking step program, leading to the fragmentation of the PrP^{Res} aggregates into smaller conversion-competent seeds. After a lag phase, the RT-QuIC product, containing β-sheet structures, may interact with the fluorescent Th-T dye, increasing the fluorescence signal. The increase of the fluorescence signal is monitored in real-time using a fluorescence plate reader. Semi-quantitative parameters such as a lag phase, the area under the curve, and maximal signal intensity can be measured to evaluate the seeded conversion efficiency [86–88]. Finally, the 96-well plate format of RT-QuIC allows automatic analysis of multiple reactions (from more than 30 different samples in triplicates), thereby facilitating the use of RT-QuIC in routine diagnostics.

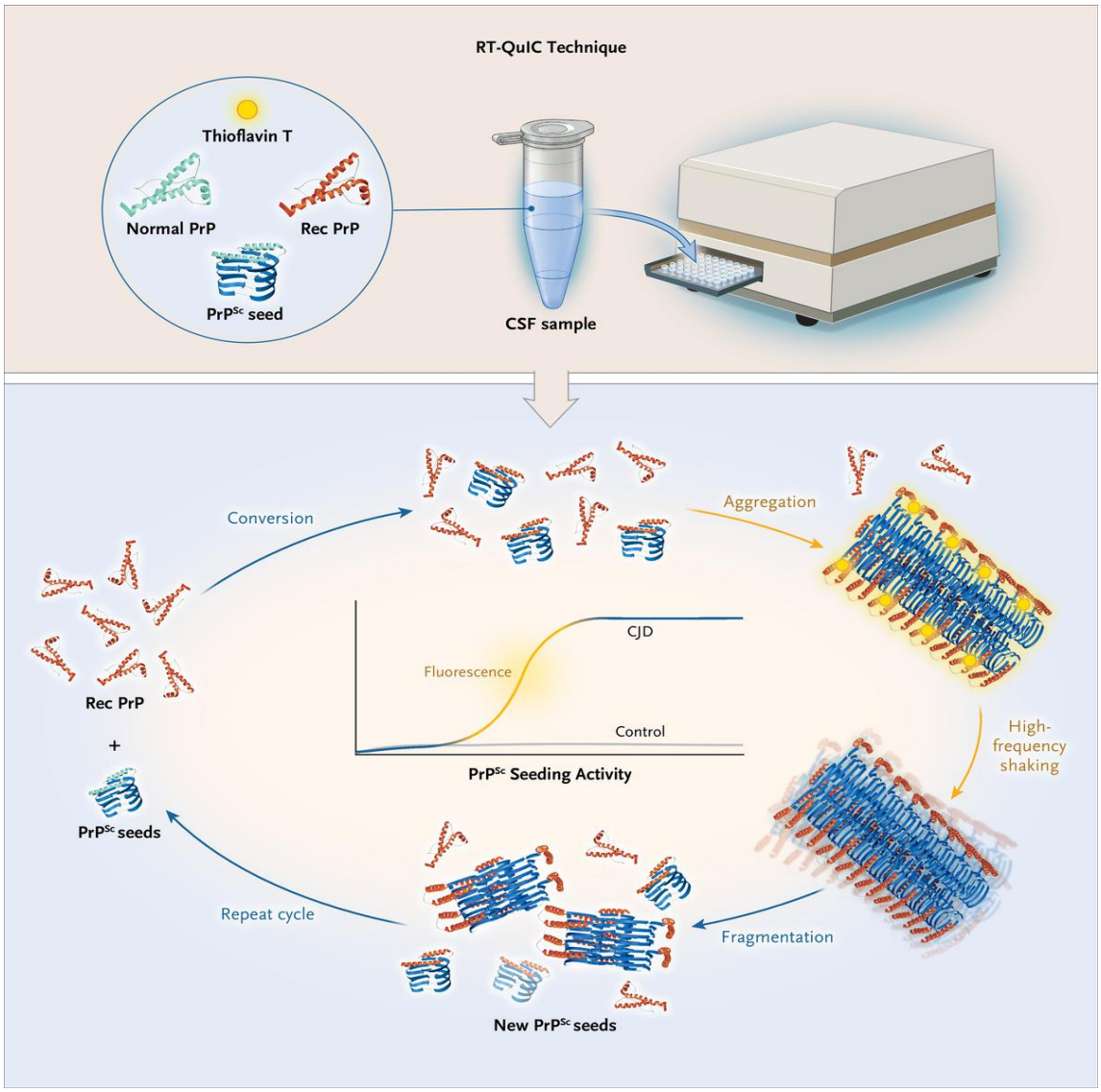

Figure 8. Detection of PrP^{Sc} on the Real-time quaking-induced conversion (RT-QuIC).

Patient's samples are mixed with the RT-QuIC basis mix, which contains rec PrP and thioflavin-T (ThT). Each sample is loaded in triplicates in a 96-well plate and placed on the RT-QuIC machine, where the samples will be subjected to intermittent cycles of incubation and shaking. The PrP^{Sc} protein from the patient sample converts the rec PrP into PrP^{Res}. The PrP^{Res} oligomers will be partially fragmented through shacking cycles, producing new seeds. In the incubation cycles, these new seeds will convert the rec PrP into PrP^{Res}, and the oligomers will continue to elongate up to the status of fibrils. These fibrils will bind to the Th-T and will produce fluorescence. This fluorescence is monitored in real-time. Positive samples for PrP^{Sc} will show a characteristic sigmoidal curve, while samples without contamination of PrP^{Sc} will not show any fluorescence increment. Figure taken from Zerr (2022) [89].

3.4 Cerebrospinal fluid (CSF) and biomarkers

Cerebrospinal fluid (CSF) is a clear and colorless water fluid secreted predominantly by a structure called choroid plexuses (CP) in the lateral, third, and fourth ventricles. CSF flows from the ventricle to the cranial and spinal subarachnoid spaces, and its absorption into the bloodstream occurs in the superior sagittal sinus through arachnoid granulations (Figure 9) [90]. It performs vital functions, including hydromechanical protection of the central nervous system. For example, it protects the brain against impact and reduces the pressure at the base of the brain by reducing the net weight of the brain from 1,400 g to 50 g (buoyancy). Additionally, CSF regulates the homeostasis of cerebral interstitial fluid and the neuronal environment by regulating the electrolyte balance, circulation of active molecules, transport of the CP secretion products to their sites of action, and elimination of catabolites. [91–93]. In a healthy condition, CSF pressure and composition remain constant. However, in many neurological diseases, its composition, pressure, and amount may be altered [94]. Measuring the levels of CSF components (CSF biomarkers) might help diagnose neurological conditions, their stages, and subtypes. The term biomarker refers to any substance, process, or structure that can be measured accurately and reproducibly as an indicator of the patient's medical state [95].

14-3-3 and total tau (tau) protein level are the CSF biomarkers that have proven to be the most valuable biomarkers to help in the probable CJD diagnosis. 14-3-3 protein is the best biomarker [96–98], with an average sensitivity of 92 % in patients with a disease duration of less than a year. Although, the sensitivity of the 14-3-3 biomarker decreased in patients with a disease duration above a year and patients with PrP^{Sc} type 2 resistant core decreasing the sensitivity to 57-84 % [99]. In addition, the measurement of CSF Tau levels by Enzyme-Linked Immunosorbent Assay (ELISA) has demonstrated its utility in supporting the diagnosis of probable CJD when used in conjunction with 14-3-3 protein detection with sensitivity of 85 % and specificity of 82 % [98].

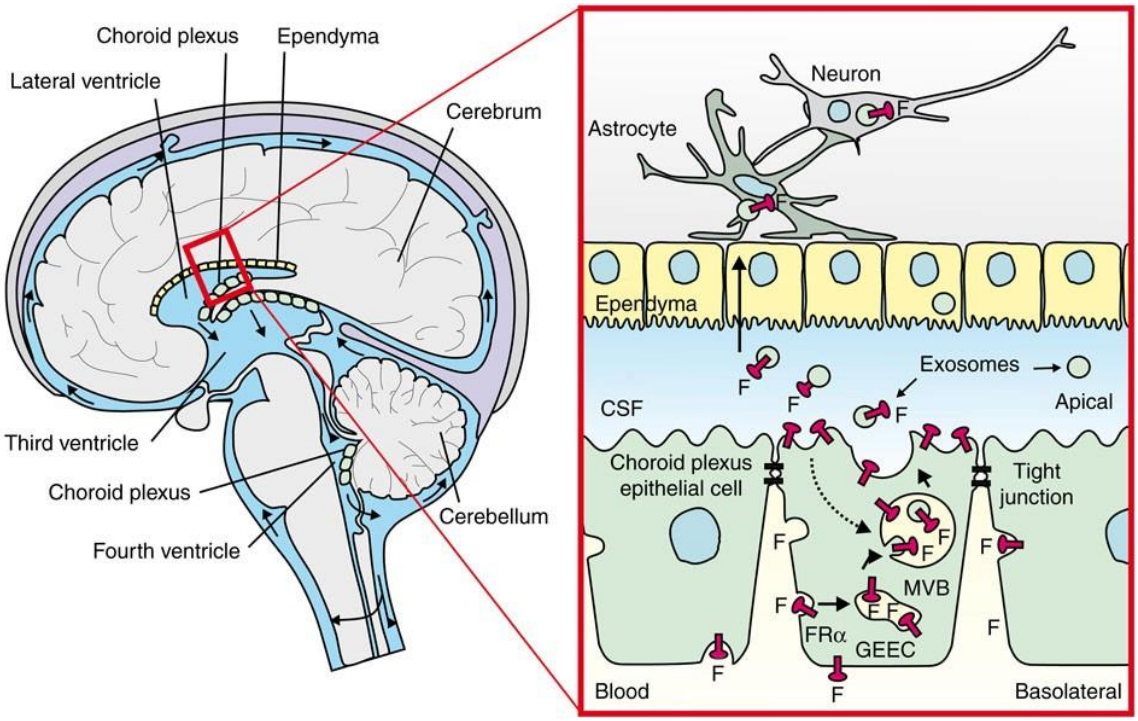

Figure 9. Schematic drawing of the brain including the cerebrospinal fluid circulation.

Figure taken from Grapp *et al.* (2013) [100].

4. Genetic forms of prion disease

Genetic forms of prion disease are rare, accounting for about 10 %-15 % of all cases of CJD. This group of CJD includes the familiar CJD (fCJD), also known as genetic CJD (gCJD), Gerstmann-Sträussler-Scheinker syndrome (GSS), and fatal familial insomnia (FFI) [101–105]. These forms of CJD are associated with pathogenic *PRNP* gene mutations, which consist of point mutations leading to amino acid substitution, premature stop codon, insertion or deletion of octapeptide repeats (OPR) in the N-terminal region of the *PRNP* (Figure 10) [106]. While some mutations are rare and associated with specific geographic and ethnic clusters, others, such as E200K (gCJD), are more worldwide distributed (Fig.11) [107,108]. In the case of sCJD or infection CJD (vCJD and iCJD), the normal form of PrP^{C} undergoes a conformal structural change into pathological conformation (PrP^{Sc}). Conversely, in genetic forms of CJD, a pathogenic mutation in the *PRNP* gene that leads to a structural alteration of the PrP^{C} is known to promote the

conformal change of this mutant PrP^{C} into PrP^{Sc} [109]. However, not all mutation carriers develop prion disease. The penetrance for the genetic form of prion disease varies between different mutations and geographic and ethnic clusters [110]. For instance, the penetrance for the gCJD with E200K mutation was 67 % in Italian [48], 59,5 % Slovak [111,112], and 100 % in the Libyan Jewish population in Israel [113].

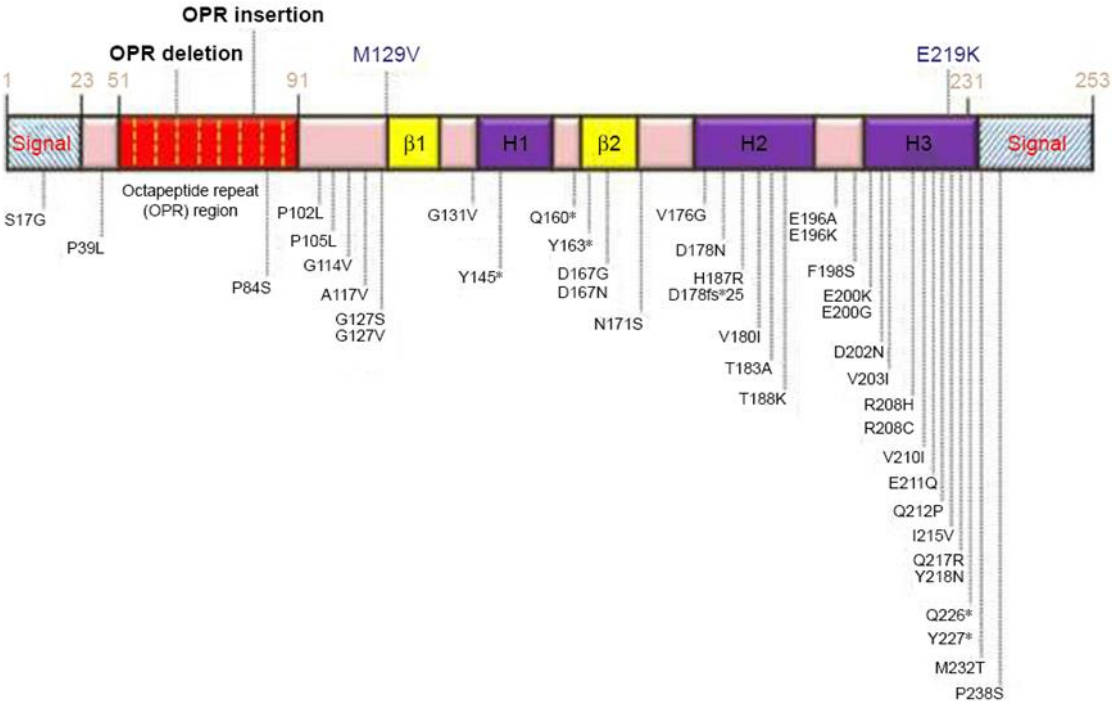

Figure 10. The human prion protein gene (*PRNP*) with all definite and suspected pathogenic mutations currently identified, colored by their predominant disease phenotype.

Figure taken from Bagyinszky *et al*. (2018) [114].

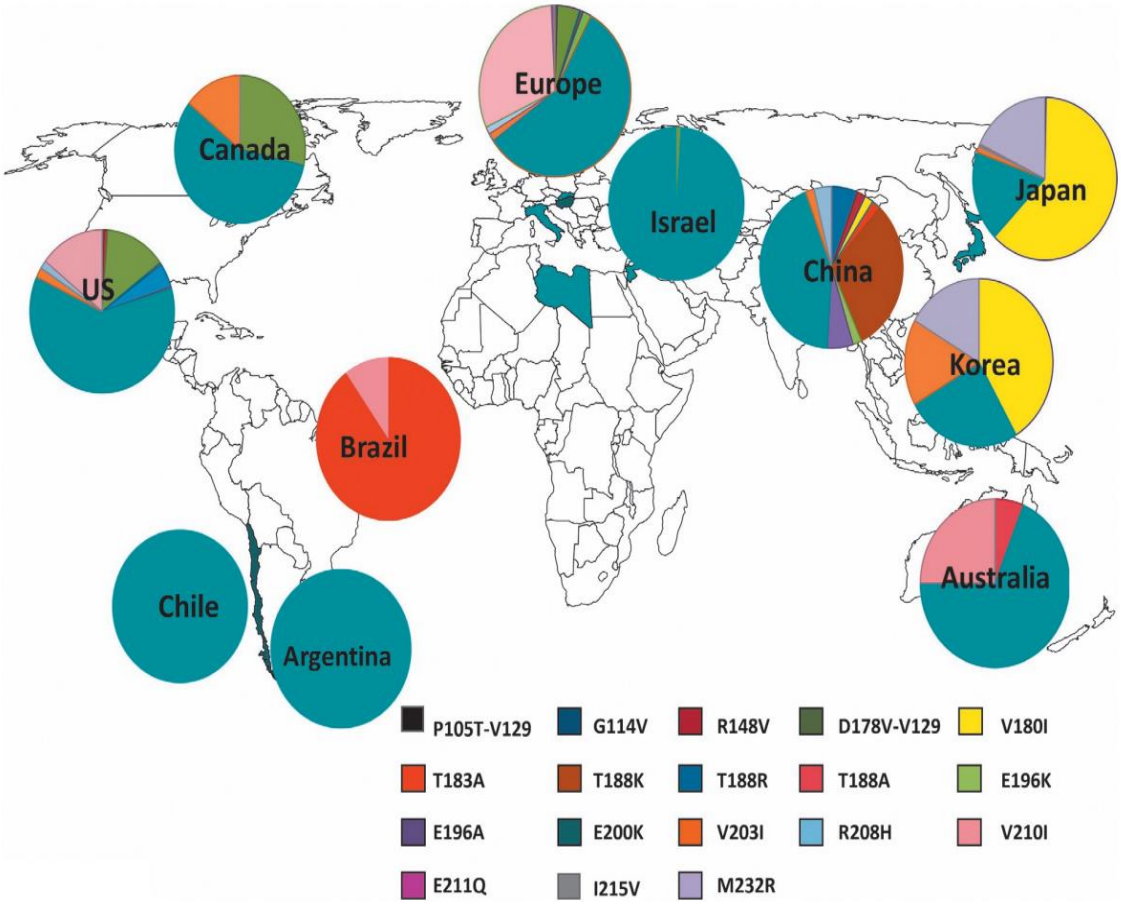

Figure 11. Worldwide distribution of *PRNP* point mutations linked to genetic Creutzfeldt–Jakob disease (CJD) in countries with CJD surveillance systems.

The countries where geographic cluster/high incidence of E200K mutation cases was reported are colored in dark blue. Figure taken from Ladogana *et al*. (2018) [115].

4.1 gCJD E200K and diagnosis

gCJD E200K is the most prevalent inherited prion disease associated with a mutation in the *PRNP* gene that leads to a substitution of lysine (K) for glutamate (E) amino acid at codon 200 (E200K) [116]. The mean age of onset is 59,3±8,4 (range 44–79) years old and the illness duration is around 7,3±6,9 (range 2–20) months [117]. The clinical feature of E200K gCJD patients are similar to the sCJD cases with the most of patients showing presence of 14-3-3 protein in the immunoblotting and elevated Tau protein in the CSF. The MRI and special PSWC on the EEG have also shown the same typical abnormalities as in the sCJD cases [118].

4.2 Fatal familiar insomnia (FFI) and diagnosis

Fatal familial insomnia (FFI) is an inherited prion disease associated with a mutation in the *PRNP* gene that leads to an exchange of aspartate (D) for asparagine (N) amino acid at codon 178 (D178N) in patients with M at the codon 129. The presence of the M at the codon 129 distinguished FFI from the fCJD patient's group with the same mutation (D178) but with V instead of M at the codon 129 [119]. Although the D178N mutation promotes the development of FFI disease, the reason for the spontaneous misfolding of PrP^{C} with the D178N mutation is still unknown. At the moment, 131 cases of FFI have been identified worldwide, with a mean age onset of 47.51±12.53 (range 17–76) years old and illness duration of 13.20±9.04 (range 2–48) months [120]. Severe sleep disorders, disturbances of the autonomic nervous system (tachycardia, hypertension, hyperhidrosis, hyperthermia), and motor signs associated with thalamic degeneration and with the progression of the disease, the neurodegeneration expands to the other brain regions are clinically characteristic of the FFI group. Although the main symptoms in FFI patients are insomnia, rapidly progressive dementia, and hypertension with a frequency of 86,7 %, 84,4 %, and 33,6 %, respectively [121]. Early clinical diagnosis of FFI remains challenging due to the high clinical heterogeneity of the disease, which could lead to an overlapping of the clinical profile of other prion diseases, such as CJD and GSS [122,123]. FFI patients rarely demonstrate PSWC on EEG (3 % sensitivity), and hyperintensity on DWI (1,1 % sensitivity) is typically absent in MRI [121]. CSF biomarkers such as 14-3-3 and Tau are typical negative (13 and 18 %), and the best CFS test performer was the RT-QuIC with a sensitivity of 28 % [82,124]. However, FFI patients can be diagnosed as a probable, possible, or definitive case of FFI when they fulfill the clinical diagnostic criteria for FFI (Figure 12) and when CJD and other neurodegenerative diseases have been ruled out through MRI, EEG, and other biomarkers.

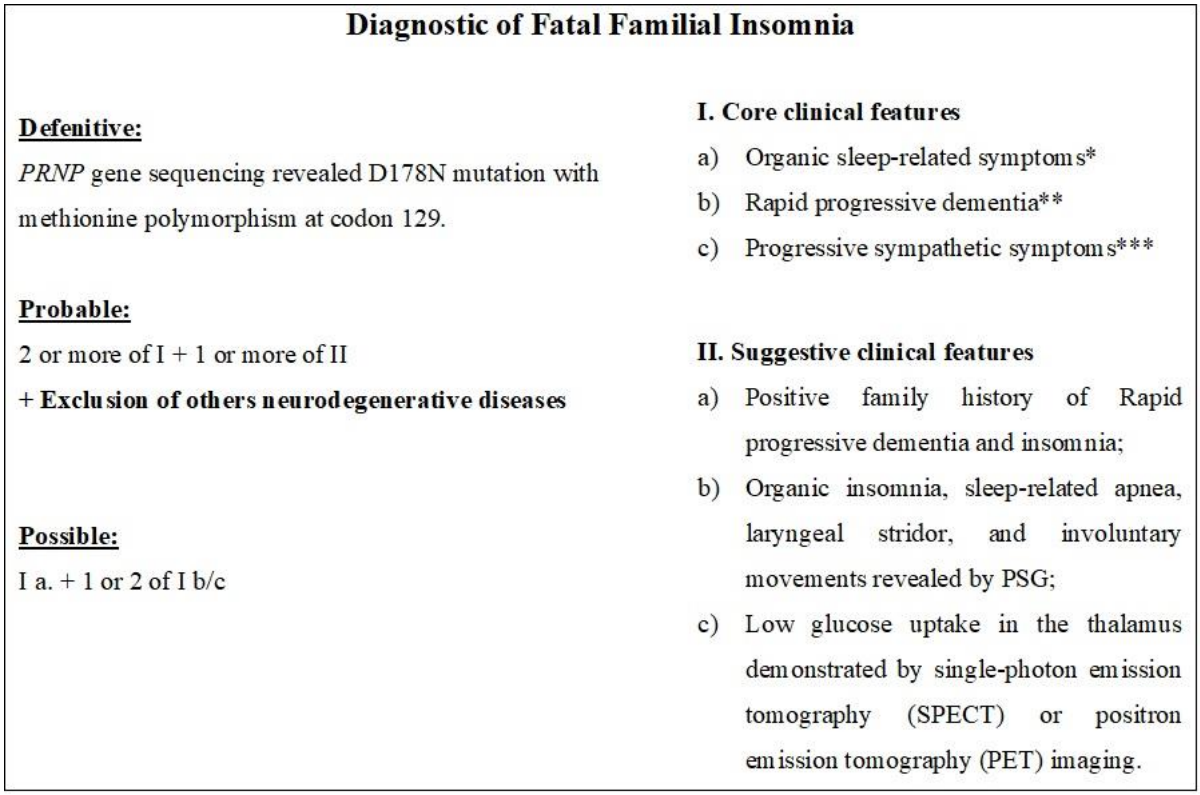

Figure 12. Criteria for the clinical diagnosis of Fatal Familial Insomnia.

The figure has been adapted from Wu L *et al* [125].

* Organic sleep-related symptoms: Insomnia, lack of deep sleep, sleep fragmentation and reduction or loss of REM sleep, laryngeal stridor, sleep breath disturbance, and involuntary movements.

** Rapid progressive dementia: The presence or absence of ataxia, pyramidal or extrapyramidal symptoms or signs, and psychiatric symptoms.

*** Progressive sympathetic symptom: Hypertension, sweating, tachycardia, and irregular breathing.

Positron emission tomography (PET), single-photon emission tomography (SPECT).

II. Aims of the project

RT-QuIC is a highly sensitive and specific diagnostic test for CJD, with a current sensitivity of 80-89 % and a specificity of 99-100 % in CSF sCJD samples conducted at the German National Reference Center for TSE [65,82]. However, in some gCJD mutation carriers and FFI patients, the sensitivity of the RT-QuIC only presents a poor sensitivity, such as 28 % in FFI cases [124]. This project aims to increase the sensitivity of the CSF RT-QuIC in CJD and FFI samples and additionally in a less invasive biological fluid (tear fluid) derived from sCJD patients. Based on these objectives, the following tasks were formulated:

1. Synthesis and purification of rec PrP substrates containing a DNA sequence of chimeric hamster-sheep, full-length human (FL Hu), FL Hu with E200K mutation (E200K) and with D178N mutation via fast protein liquid chromatography (FPLC). Afterward, we aim to define assay conditions for a reduced spontaneous self-aggregation of the substrates.

2. Signal kinetics examination of the RT-QuIC signal from different rec PrP substrates in a set of sCJD, gCJD, and FFI CSF samples (retrospective study) to identify the rec PrP substrate with the best diagnostic accuracy in the RT-QuIC essay for the detection of CJD and FFI.

3. In a prospective study, using a set of CSF samples from the routine, we aim to compare the diagnostic concordance of the routinely used hamster-sheep substrate with the FL Hu and FL Hu E200K rec PrP substrates in the RT-QuIC assay.

4. Analysis of the different RT-QuIC products from the different rec PrP through transmission electron microscopy to investigate the structural features of the aggregates in a different disease group.

5. Adaptation of the RT-QuIC protocol to detect PrP^{Sc} in a less invasive biological fluid, tear fluid, and determination of diagnostic accuracy.

III. Materials

1. Instruments and materials

The description of the instruments and materials used in this study is in Table 2.

Table 2. List of instruments used in this study.

Instrumentation	Model or Description	Manufacture
Äkta purifier	-	GE Healthcare/Amersham Biosciences
Äkta column	#XK26	GE Healthcare Life Sciences
Äkta column	#XK16	GE Healthcare Life Sciences
NanoDrop 1000 UV Visible Spectrophotometer	-	Thermofisher, USA
SnakeSkin Dialysis Tubing	10K molecular weight cut-off	Thermofisher Scientific, USA
FLUOStar Omega fluorescent reader	FLUOstar® Optima	BMG labtech, USA
Black96-well plate with bottom optic	-	Thermofisher, USA
Sealing tape, clear polyolefin	-	Thermofisher Scientific, USA
Ice machine	-	Ziegra /Isernhagen, Germany
pH meter	pH 526	WTW/ Weilheim, Germany
Pipette 0,5 -10 µl	Research plus 0,5-10	Eppendorf
Pipette 2 -20 µl	Research plus 2-20	Eppendorf
Pipette 10 -100 µl	Research plus 10-100	Eppendorf
Pipette 20 -200 µl	Research plus 20-200	Eppendorf
Pipette 100 -1.000 µl	Research plus 100-1000	Eppendorf
Serological pipettes	2, 5, 10, 25ml	Sarstedt /Germany
Safe-Lock tubes	0.2, 0.5, 1.5 and 2ml	Eppendorf /Hamburg, Germany
Conical Sterile Polypropylene Centrifuge Tubes	15 and 50ml	Sarstedt /Germany
Balance 0.01 g	CP 3202 P	Sartorius
Balance 0.001 g	TE313S-DS	Sartorius
Vortexer	Genie 2™	Bender and Hobein /Zurich, Switzerland
Homogeniser in Ultrasonic Technology	HD 2070	Bandelin Sonopuls, Germany
Centrifuge	5415C	Eppendorf/Hamburg, Germany
Amicon Ultracentrifugal 100kDa filter	100kDa filter	Merck-Millipore, IRL
Amicon Ultracentrifugal 30kDa filter	30kDa filter	Merck-Millipore, IRL

Steriflip-GP, 0,22 µm, Polyethersulfon, gamma-sterilisier	0,22 µm	Merck-Millipore, IRL
Stericup-GP, 0,20µm, Polyethersulfon, 500 ml, gamma-sterilisier	0,20µm	Merck-Millipore, IRL
Shakers	CERTOMAT R	Sartorius/ Goettingen, Germany
Thermomixer	5436	Eppendorf/ Hamburg, German
Incubator	IFE 400	Memmert/ Schwabach, Germany
ChemiDoc XRS+	-	Bio-Rad, USA
Trans-Blot Turbo transfer system	-	Bio-Rad, USA
Polyvinyldiene fluoride membrane	-	Healthcare Life Sciences, DE

2. Consumables

The description of the consumables used in this study is in Table 3.

Table 3. List of consumables used in this study.

Consumables	Abbreviation	Manufacture
Sodium chloride	NaCl	Sigma-Aldrich, USA
Ethylenediaminotetraedric acid	EDTA	Sigma-Aldrich, USA
Thioflavin-T	ThT	Sigma-Aldrich, USA
Loading buffer	-	Roth GmbH, DE
Acrylamide	-	Roth GmbH, DE
Methanol	-	Merk, DE
Tris-HCL	-	Roth GmbH, DE
Glycine	-	Roth GmbH, DE
Dry milk	-	Roth GmbH, DE
Nickel (II) chloride hexahydrate	-	Sigmaaldrich
Ni-NTA Superflow (500 ml)	-	Qiagen
Guanidine hydrochloride	-	Sigma
Sodium phosphate monobasic	-	sigma
Sodium phosphate dibasic	-	sigma

3. Bacterial cell culture

The description of the bacteria culture consumables used in this study is in Table 4.

Table 4. List of bacteria culture consumables used in this study.

Consumables	Abbreviation	Manufacture
E. coli Rosetta (DE3)	-	Merck Millipore, USA
Super optimal broth with catabolite repression	SOC	Invitrogen, USA
Tryptone/peptone from casein, granulated	-	Roth GmbH, DE
Yeast Extract	-	Roth GmbH, DE
Agar-Agar, BioScience, granulated	-	Roth GmbH, DE

4. Vectors

The list of vectors used in this study is in Table 5.

Table 5. List of vectors used in this study

Vector	Sequence	Manufacture
pET41a(+)	FL Hu PrP (23-230)	Biocat, Germany
pET41a(+)	FL Hu PrP (23-230) mutation D178N	Biocat, Germany
pET41(+)	FL Hu PrP (23-230) mutation E200K	Biocat, Germany
pET-11a	Hamster-sheep	GenScript, USA

5. Antibiotics

The list of antibiotics used in this study is in Table 6.

Table 6. List of antibiotics used in this study.

Name	Concentration	Manufacture
Chloramphenicol	> 98 %	Sigma, USA
Kanamycin solution from Streptomyces	50mg/ml in 0.9% NaCl	Sigma, USA
Ampicillin	>97 %	Roth GmbH, DE

6. Kits

The list of the kits used in this study are in Table 7.

Table 7. List of kits used in this study.

Name	Manufacture	Application
Overnight Express Autoinduction System 1 - Novagen	Merck Millipore	Protein expression
BugBuster® Master Mix	Merckmillipore	Inclusion bodies purification

7. Antibodies

The list of antibodies used in this study is in Table 8.

Table 8. List of antibodies used in this study.

Primary Antibody	Origin	Dilution IB	Manufacture
3F4 PrP	Mouse IgG2a	1:1000	Chemicon/MAB1562
SAF70	Mouse IgG2a	1:1000	Bertin Pharma
SAF32	Mouse IgG2a	1:1000	Bertin Pharma
GAPDH	rabbit IgG	1:1000	mAbcam 9484

8. Stock solutions

8.1 Electrophoresis

Electrophoresis buffer (SDS-running buffer): 192 mM glycine, 0,1 % SDS, 25 mM Tris-HCl pH 8,3.

8.2 Western blotting

TBS-T: TBS and 0,1 % of Tween-20.

Blocking solution: 5 % Milk Powder in TBS-T.

Transblot buffer for PVDF membrane (semi-dry): 192 mM Glycine, 10 % methanol, 25 mM Tris-HCl pH 8,3.

8.3 Bacteria culture

Chloramphenicol 34 mg/ml stock: 170 mg of Chloramphenicol in 5 ml ethanol. Store at -20 °C.

Ampicillin 100 mg/ml Stock: 500 mg in 5 ml deionized water (dH_2O). Filter sterilize and store at -20 °C.

Growth media Luria-Bertani (LB): 10 g Tryptone, 5 g Yeast extract, 10 NaCl. Bring to 950 ml volume, adjust pH to 7,5 with 1N NaOH and bring to 1 L of ddH_2O. Autoclave and store at room temperature.

Growth media Luria-Bertani (LB) plates: 10 g Tryptone, 5 g Yeast extract, 10 NaCl, 15 g Agar. Bring to 950 ml volume, adjust pH to 7,5 with 1N NaOH and bring to 1 L of ddH_2O. Autoclave and store at room temperature.

8.4 Protein purification

Sodium Phosphate 0,2 M Monobasic Stock: 24 g Anhydrous Sodium in 1 L H_2O. Store at 4 °C.

Sodium Phosphate 0,2 M Dibasic Stock: 28,4 g Anhydrous Sodium in 1 L H_2O. Store at 4 °C.

6 M Denaturing buffer pH 8,0: 100 mM Sodium Phosphate (142,1 ml 0,2 M Dibasic, 7,96 ml 0,2 M Monobasic), 10 mM Tris (0,3634g Tris), 6 M Guanidine (171,9 g) adjust the pH to 8,0 and bring to 300 ml with ddH_2O.

8 M Denaturing buffer pH 8,0: 38 g Guanidine in 100 mM Sodium Phosphate pH = 8,0 to a final volume of 50 ml.

Refolding buffer pH 8,0: 100 mM Sodium Phosphate (284,1 ml 0,2 M Dibasic, 15,9 ml 0,2 M Monobasic), 10 mM Tris (0,7268g) in 600 mL H_2O (total volume).

Elution Buffer pH 5,8: 100 mM Sodium Phosphate (20 mL 0,2 M Dibasic, 230 ml 0,2 M Monobasic), 10 mM Tris (0,6056 g), 500 mM Immidizole (17,017 g) adjust the pH to 5,8 and bring to 500 ml with H_2O.

Dialysis buffer pH 5,8: 10 mM Sodium Phosphate (14,3 ml 0,2 M Dibasic, 166 ml 0,2 M Monobasic), check pH (5,8) and bring to 3,6 L volume with H_2O.

9. Ethics Statement

The studies involving human CSF and tear fluid samples were reviewed and approved by the local Ethics Committee of the University Medicine Göttingen, Von Siebold-Str., 37075 Göttingen, No. 24/8/12. All samples were analyzed blindly for at least personal data.

10. CSF samples

All suitable CSF samples, without contamination with blood, were stored at -80°C before analyses. The list of the CSF samples used in this study is in Table 9.

Table 9. List of CJD CSF samples used in this study.

The table recapitulates the clinical features (genotype, histopathologic type, mutation, sex, and age of death) of the patients used in this study.

Genotype	**Gender (F/M)**	**Age at onset**	**CJD Diagnose (Prob./ Def.)**
MM	5/9	66±11	7/7
MV	7/5	59±10	9/3
VV	4/7	53±14	4/7
Subtype	**Gender (F/M)**	**Age at onset**	**CJD Diagnose (Prob./ Def.)**
MM1/MV1	18/20	68±9	1/37
VV2	3/5	66±10	1/7
Mutation	**Gender (F/M)**	**Age at onset**	**CJD Diagnose (Prob./ Def.)**
E200K	10/7	59±1	0/17
D178N	8/14	52±15	0/22
Without genotype or subtype	**Gender (F/M)**	**Age at onset**	**CJD Diagnose (Prob./ Def.)**
sCJD CSF	5/9	69±15	9/0

11.Tear fluid samples

All tear fluid samples from patients diagnosed with CJD, were stored at -80 °C before analyses. The list of the CSF samples used in this study is in Table 10.

Table 10. List of tear fluid samples used in this study.

The table recapitulates the clinical features (genotype, mutation, sex, and age) of the patients used in this study.

Gender	Age	Mutation	Genotype	Biopsy	CSF RT-QuIC
Female	42	FFI	MM	-	-
Female	44	GSS	-	-	-
Female	47	-	-	yes	-
Male	55	FFI	-	-	-
Male	68	-	-	-	Pos 2/3
Male	53	-	-	-	Pos 3/3
Female	38	-	-	-	-
Male	60	-	-	-	-
Male	36	GSS	-	-	-
Male	58	-	MV	-	-
Female	64	-	-	-	-
Male	69	-	MM	-	Pos 3/3
Female	79	-	-	-	Pos 2/3
Female	72	-	-	-	-
Female	59	-	-	-	-
Female	39	T183A	MV	-	-
Male	70	-	MM	-	-
Male	63	-	-	-	Pos 3/3
Female	71	-	-	-	Pos 3/3
Female	43	T183A	MV	-	-
Female	79	-	-	-	Pos 3/3
Female	68	-	-	-	Pos 3/3
Male	63	-	-	-	Pos 2/3

IV. Methods

1. Vector construction and transformation in *E. coli* Rosetta cells (DE3)

The constructed pET41a (+) vectors encoding Human PrP 23-230 (residues 23 to 231), Human 23-230 with E200K mutation, Human 23-230 with D178N mutation (Biocat, Germany), and pET-11a vector encoding chimera recombinant PrP composed of Syrian hamster residues 14 to 128 followed by sheep residues 141 to 234 of the R154 Q171 polymorph [126] (GenScript, USA), all vectors without a C-terminal 6-His-tag were transformed into expression host *E. coli* Rosetta cells (DE3) (Merck Millipore, USA) according to the manufacturer's instructions. 20 µl of *E. coli* Rosetta (DE3) cells were thawn on ice until the last ice crystal disappeared, around 10 min. 1 µl containing approximately 1 to 10 ng/µl plasmid DNA in TE buffer (10 mM Tris-HCl, 1 mM EDTA, pH 8,0) was directly added to the bacteria cells and left on ice for 5 min. The cells were heat-shocked at 42 °C for 30 s and placed on ice for 2 min before adding 80 µL super optimal broth with catabolite repression media (SOC) (Invitrogen, USA). The cells were shaken at 250 RPM at 37 °C for 60 min before spreading 50 µl on Luria-Bertani (LB) agar plates containing 50 µg/ml kanamycin (*E. coli* Rosetta cells (DE3) transfected with pET41a (+) vector) or 100 µg/ml ampicillin (*E. coli* Rosetta cells (DE3) transfected with pET-11a) with 34 µg/ml chloramphenicol (*E. coli* Rosetta cells (DE3) are resistant to chloramphenicol). Afterwards, the plates were incubated overnight at 37 °C.

2. Bacteria culture and protein expression

A single colony from an overnight LB agar plate was picked and added to the 4 ml LB medium with 50 µg/ml kanamycin (pET41a (+) vector is resistant to kanamycin) or 100 µg/ml ampicillin (pET-11a vector is resistant to ampicillin) with 34 µg/ml chloramphenicol in a 50 ml falcon tube. 2 mini cultures were prepared and incubated at 37 °C, 250 rpm for 6 h. For protein overexpression, it was added an Overnight Express Autoinduction system 1 (Sigma Aldrich**,** USA) to 1 L of LB medium with kanamycin (50 µg/ml) or ampicillin (100 µg/ml) and chloramphenicol (34 µg/ml) antibiotics before the addition of the mini cultures. The cells were then shaken at 250 RPM at 37 °C for 20 h, centrifuged (10000 x g for 10 min), and the supernatant discarded. The pellet was

weighted (±16 g per 1 L) and stored in 50 ml Falcon tubes (4 Falcon tubes with ±4 g each) at -20 °C overnight or -80 °C until further use.

3. Inclusion Bodies Purification

The inclusion bodies were purified using BugBuster Mix (Merck Millipore, USA) according to the manufacturer's instructions with slight modifications. Each of the 4 Falcon tubes containing ±4g bacteria pellet was placed on ice to thaw for 30 min before being resuspended by pipetting up and down and homogenized (Bandelin Sonopuls, Germany) with 14 ml room temperature 1X Bug Buster Master Mix (Merck Millipore, USA) for 1 min, 5 cycles at 45 % power. Each bacteria cell suspension was incubated on a rotating mixer at room temperature for 20 min, followed by centrifugation at 13,000 x g for 20 minutes at 4 °C. The supernatant was discarded, and the bacteria pellet resuspended in 14 ml 1X Bug Buster Master Mix using the same pipette as before and re-homogenized (1 min, 5 cycles at 45 % power) before incubation at room temperature for 20 min. After 20 min, 0,1X Bug Buster Master Mix (Merck Millipore, USA) was added to the cell suspension until it reached the total volume of 40 ml before centrifugation (13,000 x g, 15 min at 4 °C). Afterwards, the supernatant was discarded. The pellet was resuspended by pipetting up and down with 30 ml room temperature of 0,1X Bug Buster Master Mix (Merck Millipore, USA) before centrifugation (8,000 x g, 15 min at 4 °C). After centrifugation, the supernatant was discarded, and the inclusion body pellet was stored at -20°C overnight.

4. Protein Purification

Each inclusion body pellet into 50 ml Falcon tubes from the pellet of 1 L bacterial culture (total of 4 Falcon tubes per 1 L of bacteria culture) was placed on ice to thaw for 30 min before being dissolved by adding 14 ml of 8 M guanidine (38 g guanidine in 0,1M $NaPO_4$ at pH 8) and homogenized (Bandelin Sonopuls, Germany) for 1 min 5 cycles at 45 % power. Dissolved inclusion bodies suspension was incubated on a rotating mixer at room temperature for 50 min before centrifugation (13,000g, 5 min at 4 °C). After centrifugation, each supernatant was mixed with equilibrated 18 g of Ni-NTA beads in 30 ml Denaturing buffer (6M GdnHCl in 0,1M $NaPO_4$ at pH 8) for 40 min to allow the

proteins to bind to the beads. After incubation, 3x 18 g incubated resin was pulled and loaded into the Äkta #XK26 column, and 1x 18 g incubated resin was loaded into Äkta #XK16 column. The column was attached to FPLC, and the following gradient refolding program was running: 100 % A (Denaturing Buffer) and 0 % B (Refolding Buffer (0.1M NaPO4 at pH 8)) to 0 % A and 100 % B for 240 min (0,75 ml/min for #XK16 column with 18g beads and 2,20 ml/min Äkta #XK26 column with 3X 18g beads). After gradient refolding additional 30 min of 100 % B (Refolding Buffer) has flowed through the column. To elute the protein, a gradient elution program was running: 100 % A (Refolding Buffer) and 0 % B Elution Buffer (0,5M C3H4N2 in 0,1M NaPO4 at pH 5,8) to 0 % A and 100 % B for 50 min (2 ml/min for #XK16 column with 18 g beads and 6 ml/min Äkta #XK26 column with 3x 18 g beads). The fraction tubes with the eluted proteins were collected from the center of the large UV 280 peak and combined before being diluted with 1/3 volume of Dialysis Buffer at 4 °C (10mM NaPO4 at pH 5,8). The diluted protein was filtered with a sterile disposable 0,22 µm filter (Merck Millipore, USA) before being put into a SnakeSkin dialysis tubing with a 10 kDa molecular weight cut-off (Thermofisher, USA) for dialyze in 3,6 L of dialysis buffer at 4°C for 1-4 h before being transferred to a fresh 3,6 L dialysis buffer for overnight at 4 °C. After overnight, the SnakeSkin tubing was transferred into a fresh 3,6 L dialysis buffer for 4 h before the proteins were filtered once again with a sterile disposable 0,22 µm filter (Merck Millipore, USA) and the 2 batches combined (1x 18 g beads and 3x 18 g beads). The protein concentration was measured using NanoDrop 1000 UV Visible Spectrophotometer (Thermo Scientific, USA) at 280 nm before being aliquoted and stored at -80 °C.

5. Purified protein concentration estimated by NanoDrop 1000 UV Visible Spectrophotometer

The protein concentration was estimated by NanoDrop 1000 UV visible Spectrophotometer (Thermofisher, USA). Protein A280 application was selected from the main menu of the nanodrop software, and 2 µl of the dialysis buffer (10 mM Sodium Phosphate, pH = 5,8) was pipetted into the bottom pedestal for blank measurement. The blank solution (Dialysis buffer) was wiped from the lower and upper pedestals, and 2 µL of the purified protein sample was loaded onto the bottom pedestal, and the concentration

was measured. The purified protein sample was wiped from the upper and lower pedestal using a dry laboratory wipe, and 2 µL ddH_2O was added and wiped again before the subsequent sample measurement.

6. Coomassie Brilliant Blue Staining

Proteins from bacteria culture were loaded before and after overnight expression, inclusion bodies lysis, and purified protein into 12 % acrylamide gels and separated by electrophoresis. Acrylamide gels were fixed in a solution containing 50 % methanol and 10 % glacial acetic acid for 1 h. After 1 h, the solution was exchanged. Staining with 1% Coomassie brilliant blue R-250, 50 % methanol, and 10 % glacial acetic occurred for 20 min with gentle agitation. Destaining in 40 % methanol and 10 % glacial acetic acid solution was carried out until the gel background was fully transparent and destained. Finally, gels were stored at RT in a 5 % glacial acetic acid solution.

7. Immunoblot

Immunoblotting from bacteria culture before and after overnight expression, inclusion bodies lysis, and protein purification were performed. Briefly, 50 µL of bacteria cells lysed in 1x Bug Buster Master Mix (Merck Millipore, USA), 50 µL of Inclusion body suspension in 0,1x Bug Buster Master Mix, and 50 µL of purified protein were combined with 50 µL of 4x+- SDS Sample Buffer, immediately heated for 3 min at 85 °C, and the proteins were separated on 12 % acrylamide gels. The proteins from SDS-PAGE were transferred to a PVDF blotting membrane and were incubated with antibodies against PrP^C (SAF70 and SAF32 1:1000, Bertin Pharma) overnight at 4 °C. After that, the PVDF blotting membrane was washed 3 times for 30 min with 1x TBS-T and incubated with the secondary antibodies of anti-mouse in 5 % milk (1:5000) for an hour, at RT, and then washed again 3 times with 1x TBS-T. Immunoreactivity was detected after immersion of the membranes into enhanced chemiluminescence (ECL) solution for 5 min and exposure to ECL-Hyperfilm (Amersham Biosciences, Buckinghamshire, UK). Images were documented using the ScanMaker4 (Microtek, International), after correction for the background, and band intensities were determined by densitometry using Labimage (version 2.7.1, Kapelan GmbH, Germany) data analyzer software.

8. Real Time-Quaking Induced Conversion

RT-QuIC analysis was performed according to an established protocol [86]. Each CSF sample was run in triplicates and considered positive when at least two out of three replicates gave a positive seeding response (signal increase >50 %). Briefly, 15 µl of CSF sample (seed) were added in 85 µl of RT-QuIC buffer (total volume of 100 µl in each well of 96-well plate), containing 57 µl of basis mix (1x PBS, pH 6.9, 170 mM NaCl, 1 mM EDTA), 1 µl of 1 mM Th-T and 27 µl rec PrP^C (0.37 mg/ml). Reactions were prepared in a black 96-well plate with a bottom optic covered with sealing tape (Thermo-Fisher Scientific, USA) and incubated at 42 °C using a FLUOStar Omega fluorescent reader (BMG Labtech, USA), with 1 min of double orbital shaking at 600 RPM followed by 1 min incubation. Every 30 min, fluorescence measurements (excitation 450 nanometers (nm) wavelength, emission 480 nm wavelength) were taken. The reaction was run for 161 cycles, corresponding to 80 h. RT-QuIC reactions without seed were run to estimate a potential self-aggregation from each substrate.

9. Statistical analysis

Agreement between different substrates was calculated using Cohen's kappa value. A Cohen's kappa value of 0,01-0,20 was defined as a slight agreement, 0,21-0,40 fair agreement, 0,41-0,60 moderate agreement, 0,61-0,80 substantial agreement, 0,81-1,00 almost perfect agreement between raters. Measures of seeding effciency were calculated for each different substrate as well for each different CJD group by the relative area under the curve (rel. AUC), lag phase (time to 50 % signal increase), and maximum ThT signal. Multiple comparisons data were analyzed by one-way ANOVA followed by Dunn's Post hoc test. Two groups (normally distributed) were compared using the Student's t-test, while for non-normally distributed values, we considered the Mann–Whitney U test as appropriate. All analyses were conducted by using GraphPad Prism.

10.Transmission electron microscopy

Transmission electron microscopy images from the RT-QuIC product using different rec PrP substrates and prion diseases were possible through a collaboration with Prof. Dr. Holger Wille and PhD Razieh Kamali, University of Alberta, Canada.

11. Tear fluid samples

Insertion of a 5 mm wide and 35 mm long strip of filter paper in the outer corner of the eyelid in the conjunctival sac of the eye. After 5 min the filter paper is removed. The procedure corresponds to the standard for determining the amount of tear production (so-called Schirmer test (Figure 12) in ophthalmology. Time required: approx. 10 min.

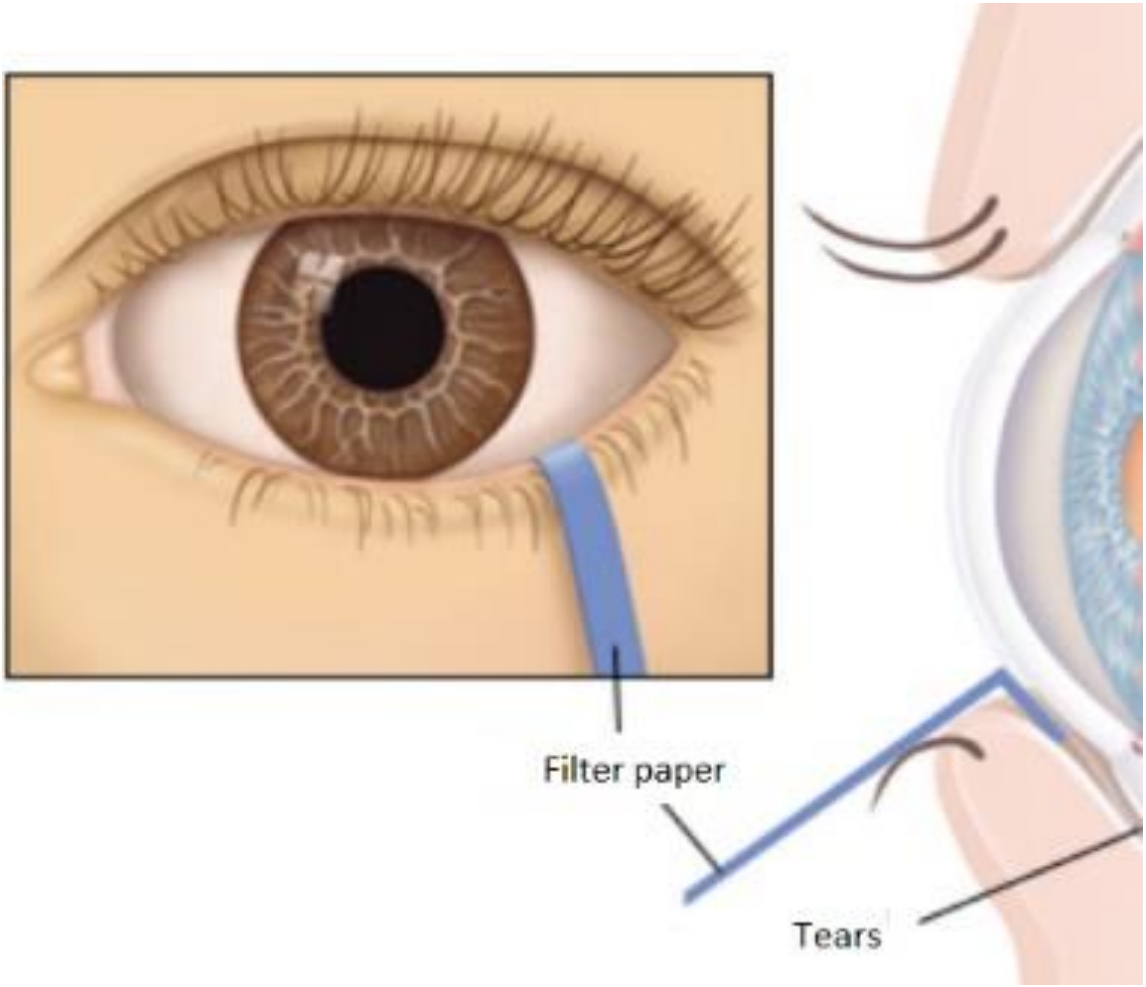

Figure 13. Schirmer's test.

V. Results

1. Analysis of a potential self-aggregation of rec PrP substrates

Before proceeding with the seeded RT-QuIC analysis of patient samples, we assayed whether different rec substrates are prone to self-aggregation. To this aim, RT-QuIC analysis with five CSF samples from non-CJD controls, five without seed (without CSF), and five without substrates was running in triplicates. All reactions with hamster-sheep, FL Hu, and FL Hu E200K substrates remained negative (Figure 14, A-C). Since rec PrP substrate containing the FFI mutation showed positive reactions with CSF controls, and without CSF, we excluded the FFI substrate for further analysis (Figure 14, D).

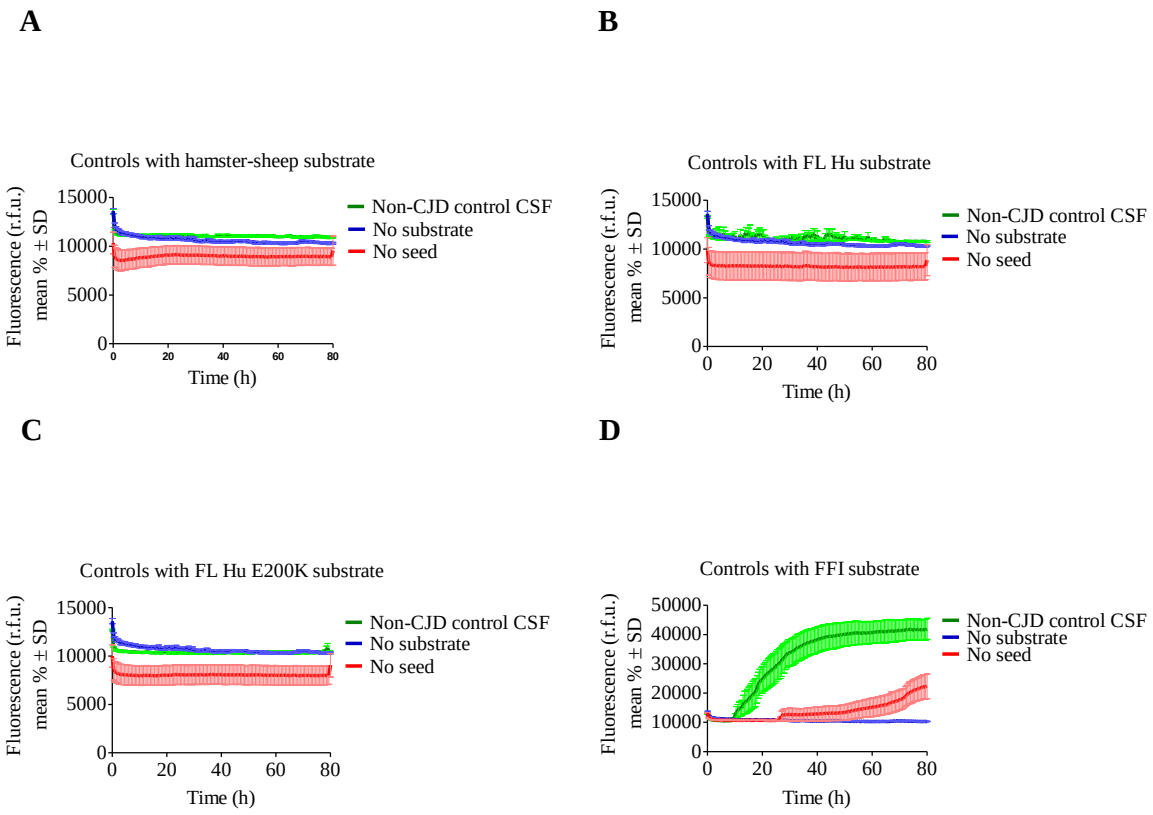

Figure 14. Fluorescent curves of the RT-QuIC reactions using hamster-sheep, FL Hu, FL Hu E200K, and FFI substrates.

Five reactions without CSF-seed (red line), five without substrate (blue line), and five with non-CJD CSF controls (green line) with hamster-sheep (A), FL Hu (B), and FL Hu E200K (C) substrate showed a negative

seeding response (flat lines) after 80 h measurement. RT-QuIC reactions using the rec PrP FFI substrate either (D) seeded with non-CJD controls CSF samples (green line) or without CSF-seed (red line) indicated self-aggregation properties of this substrate.

2. Stability of different rec PrP substrates in the RT-QuIC under defined storage conditions

To determine the stability of different rec PrP substrates in the RT-QuIC seeding reaction, five sCJD samples in triplicates were subjected to repeated freezing and thawing cycles (up to 12 times). Different time points were chosen:

As a reference we considered T0 without freezing and thawing. Further time points were selected, after four (T4), eight (T8), and twelve (T12) cycles of freezing and thawing. All five sCJD reactions with hamster-sheep, FL Hu, and FL Hu E200K substrates remained positive after 12 cycles of freezing and thawing without any significant changes in the seeding kinetics (Figure 15).

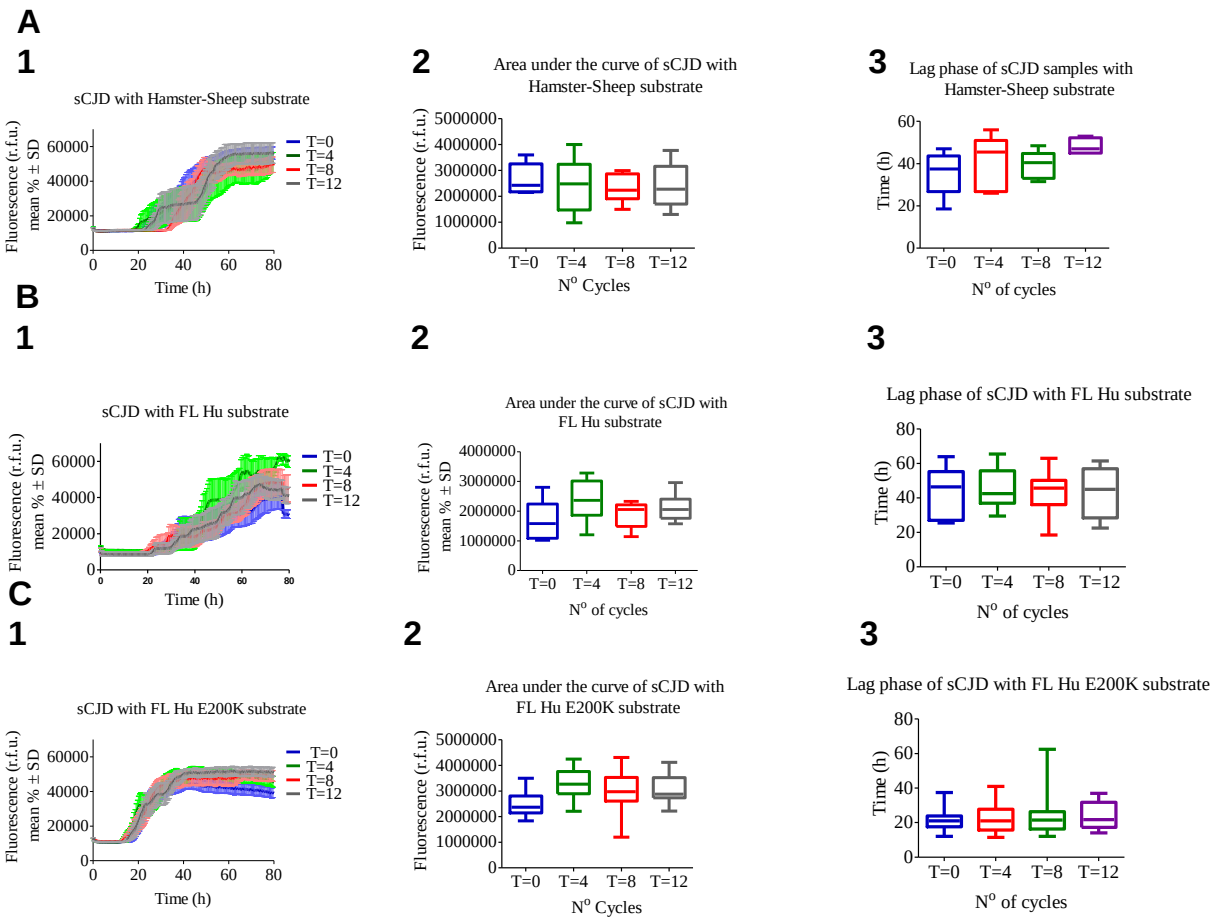

Figure 15. Resistance RT-QuIC reactions with hamster-sheep, FL Hu, and FL Hu E200K substrates to different freezing and thawing cycles.

(A,1) Mean fluorescence values (+/- SD) of five RT-QuIC reactions using Hamster-sheep substrate after the indicated freezing and thawing cycles were shown. Hamster-sheep substrate showed any significant difference in AUC (A,2) and lag phase (A,3) after twelve freezing and thawing cycles. (B,1) Mean fluorescence values (+/- SD) of five using FL Hu substrate seeded with sCJD CSF after different freezing and thawing cycles. FL Hu substrate showed significant differences in AUC (B,2) and Lag phase (B,2) after twelve cycles of freezing and thawing. (C,1) Mean of fluorescent curves (+/- SD) of the RT-QuIC reactions using FL Hu E200K substrate seeded with five sCJD CSF samples in different freezing and thawing cycles. FL Hu E200K substrate showed no significant differences in AUC (C,2) and Lag phase (C,3) after twelve freezing and thawing cycles.

3. Influence of different substrates on the intensity of RT-QuIC seeding response in sCJD

To investigate the impact of different rec PrP substrates on the RT-QuIC seeding response, 78 sCJD CSF samples and 44 non-CJD control CSF samples were subjected to RT-QuIC analysis [86]. We applied different rec PrP substrates (hamster-sheep, FL Hu, and FL Hu E200K) in the RT-QuIC assay and seeded them either with sCJD or control CSF. All the controls were negative in this study and 43 out of 78 sCJD CSF samples had been tested positive with all rec PrP substrates. The signal kinetic of the positive sCJD CSF samples (n=43) for all rec PrP substrates were quantified by following three seeding parameters of interest: lag phase, AUC, and the maximum signal of RT-QuIC response. FL Hu E200K was the rec PrP with the shortest lag phase when compared with hamster-sheep (* $p \leq 0,05$) and FL Hu substrates (*** $p \leq 0,001$). FL Hu substrate exhibited the most extended lag phase with a significant difference in comparison with hamster-sheep (** $p \leq 0,01$) and a significant difference when compared with FL Hu E200K (*** $p \leq 0,001$) (Figure 15, C). FL Hu substrate exhibited the highest maximal signal intensity in comparison with hamster-sheep (* $p \leq 0,05$) and FL Hu E200K (*** $p \leq 0,001$) substrates (Figure 16, D) and a higher AUC when compared with FL Hu E200K (*** $p \leq 0,001$) (Figure 16, B). Non-CJD control CSF samples showed negative RT-QuIC responses (no seeding conversion, defined as a fluorescence signal lower than 10,000 r.f.u.) for all substrates (Figure 16, E).

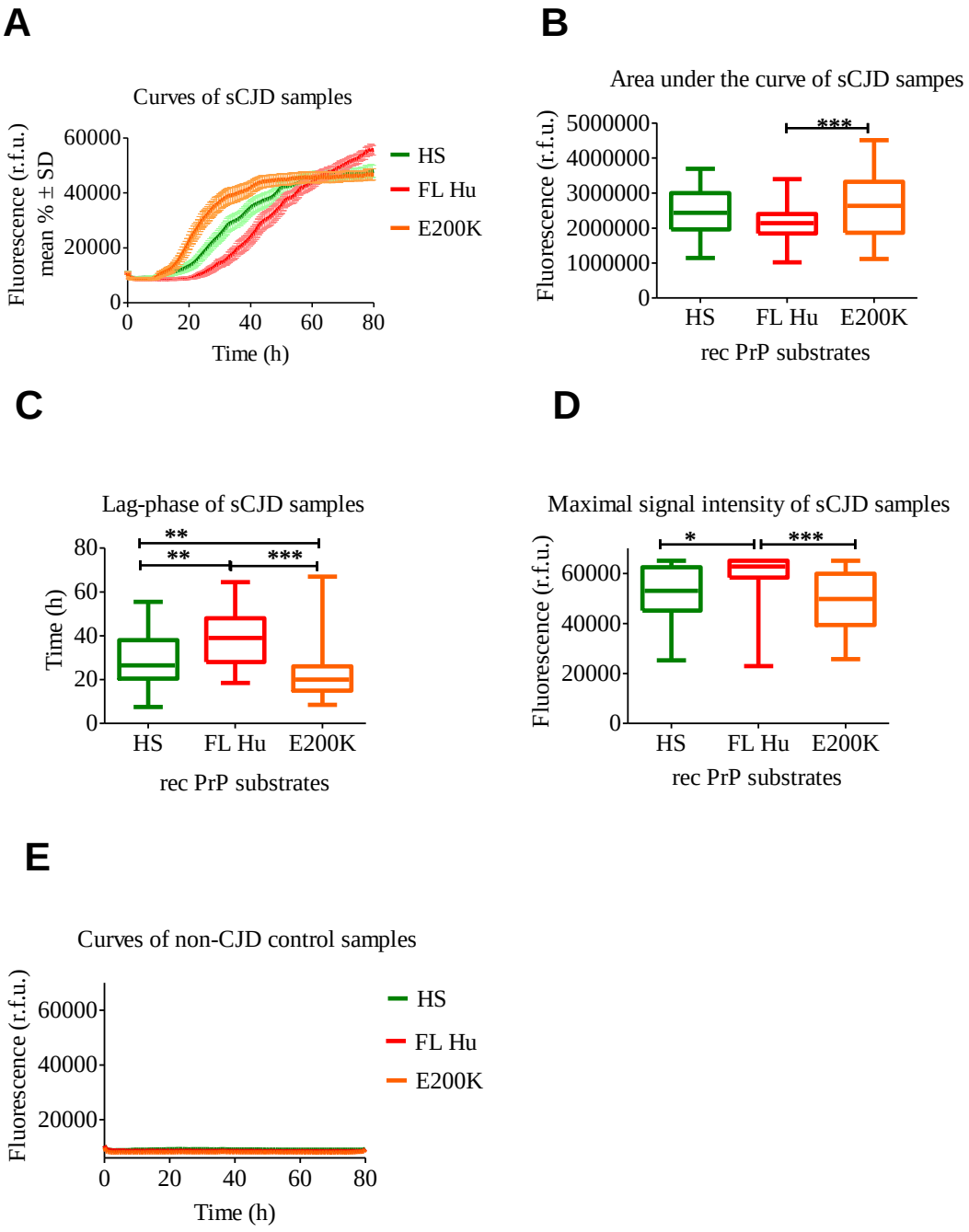

Figure 16. Influence of hamster-sheep (HS), FL Hu, and FL Hu E200K (E200K) substrates on the RT-QuIC signal response.

Positive seeding response curves of sCJD patients samples (A) were depicted for each rec PrP substrates (n=43 patients). For quantitative analysis we calculated for each substrate following three parameters of interest: AUC (B), lag phase (C), and the maximum signal maximum (D) of RT-QuIC response.

3.1 Determination of diagnostic accuracy of different rec PrP substrates in the RT-QuIC assay

To investigate the diagnostic accuracy (sensitivity and specificity) of the different substrates used in this study, we analyzed the RT-QuIC signal response of 78 sCJD CSF and 44 non-CJD CSF samples running in triplicates for each substrate. Two out of three positive RT-QuIC reactions were counted as CJD-positive. The overall sensitivity of the hamster-sheep substrate was 85 %, FL Hu substrate was 76 %, and FL Hu E200K substrate was 95 %. All substrates reveled a specificity of 100 % (n=44) (Table 11). FL Hu E200K substrate reached 100 % of sensitivity in almost all sCJD genotypes and subtypes except for the sCJD MM genotype (79 % sensitivity) (Table 12) and MM/MV1 subtype (92 % sensitivity) (Table 13).

Table 11. Overview of diagnostic accuracy in sCJD.

The table recapitulates diagnostic accuracy of hamster-sheep, FL Hu, and FL Hu E200K substrates.

		Hamster-sheep	FL Hu	FL Hu E200K
sCJD	Definitive	41/48 (85%)	39/48 (81%)	45/48 (94%)
	Probable	25/30 (83%)	20/30 (67%)	29/30 (97%)
	Total	**66/78 (84.6%)**	**59/78 (76%)**	**74/78 (95%)**
Non-CJD		**0/44 (100%)**	**0/44 (100%)**	**0/44 (100%)**

Table 12. Overview of diagnostic accuracy in different sCJD genotypes.

The table recapitulates the diagnostic accuracy of hamster-sheep, FL Hu, and FL Hu E200K according to the *PRNP* M/V genotype at codon 129.

	Hamster-sheep	FL Human	FL Hu E200K
sCJD MM	11/14 (71 %)	10/14 (71 %)	11/14 (79 %)
sCJD MV	8/12 (67 %)	9/12 (75 %)	12/12 (100 %)
sCJD VV	9/11 (82 %)	10/11 (91 %)	11/11 (100 %)

Table 13. Overview of diagnostic accuracy in different sCJD subtypes.

The table recapitulates the diagnostic accuracy of hamster-sheep, FL Hu, and FL Hu E200K according to the subtype.

	Hamster-sheep	FL Hu	FL Hu E200K
MMMV1	35/38 (92 %)	29/38 (76 %)	35/38 (92 %)
VV2	6/8 (75 %)	7/8 (87.5 %)	8/8 (100 %)
MV2K	1/2 (50 %)	2/2 (100 %)	2/2 (100 %)

4. Influence of different substrates on the RT-QuIC seeding response in genetic prion diseases

4.1 Influence of RT-QuIC substrates on the seeding conversion process of gCJD E200K

To investigate the impact of different rec PrP substrates on the RT-QuIC seeding response of gCJD E200K, 16 gCJD E200K CSF samples and 44 non-CJD controls were subjected to RT-QuIC analysis using the standard protocol [86]. As a substrate for RT-QuIC we applied rec PrP hamster-sheep, FL Hu, and FL Hu E200K. The RT-QuIC reaction's kinetic signal was measured and quantified according to the duration of the lag phase and the AUC values (Figure 17). We observed a significant shorter lag phase in reactions with FL Hu E200K as a substrate when compared with hamster-sheep (* $p \leq 0,05$) or with FL Hu substrate (*** $p \leq 0,001$) (Figure 17, C). In addition, FL Hu E200K substrate showed significant higher AUC values in comparison with hamster-sheep (** $p \leq 0,01$) and with FL Hu substrates (*** $p \leq 0,001$) (Figure 17, B). The maximum fluorescence values did not reveal any significant difference between different rec PrP substrates. Control samples without prion disease showed a negative RT-QuIC responses (<10,000 r.f.u.) for all rec PrP substrates.

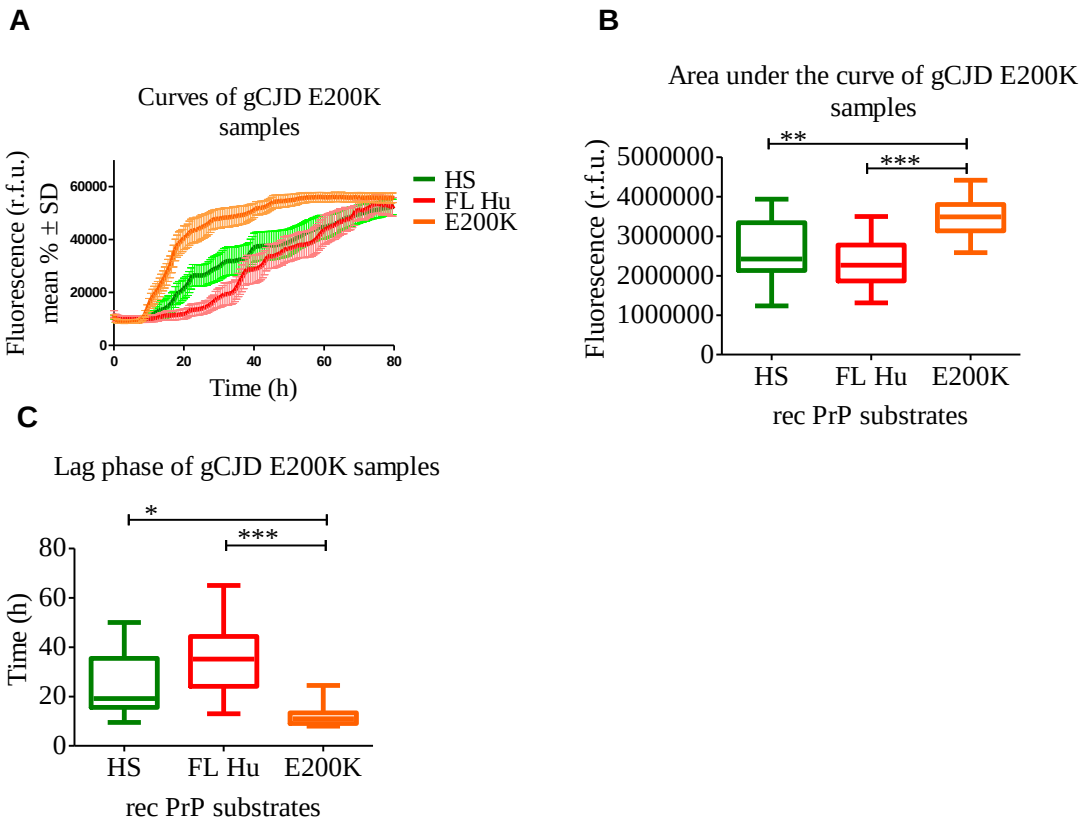

Figure 17. Influence of hamster-sheep, FL Hu, and FL Hu E200K substrates on the RT-QuIC signal response in genetic CJD E200K seeded reactions.

RT-QuIC reactions were seeded with CSF from non-CJD controls (n=44) and gCJD E200K patients (n=16). (A, B) FL Hu E200K showed an extremely significant (*** $p \leq 0{,}001$) influence on the seeding kinetic and AUC when compared with FL Hu substrate and a significant difference in comparison with hamster-sheep substrate (** $p \leq 0{,}01$). (C) FL Hu E200K increased the conversion efficiency of PrP significantly, as indicated by a short lag phase in comparison to hamster-sheep (* $p \leq 0{,}05$) and FL Hu (*** $p \leq 0{,}001$) substrates.

4.1.1 Determination of diagnostic accuracy of different rec PrP substrates in the RT-QuIC assay for gCJD E200K

To investigate the diagnostic accuracy in gCJD E200K CSF samples, we analyzed the RT-QuIC signal response of 17 E200K gCJD CSF running in triplicates for each substrate. We counted all samples with a fluorescence curve in at least two of the three RT-QuIC wells as a positive samples for gCJD. The sensitivity of the hamster-sheep

substrate was 88 %, of FL Hu substrate 88 %, and of FL Hu E200K substrate 100 % for gCJD (Table 14).

Table 14. Overview of diagnostic accuracy in gCJD E200K.

The table recapitulates the RT-QuIC results in hamster-sheep, FL Hu, and FL Hu E200K in E200K gCJD CSF samples.

	Hamster-sheep	FL Hu	FL Hu E200K
gCJD E200K	15/17 (88 %)	15/17 (88 %)	17/17 (100 %)
Non-CJD controls	0/44 (100 %)	0/44 (100 %)	0/44 (100 %)

5. Influence of RT-QuIC substrates on the seeding conversion process of FFI

To investigate the impact of different rec PrP substrates on the RT-QuIC seeding response in FFI, 22 FFI CJD CSF samples were subjected to RT-QuIC analysis using the standard protocol [86], for which rec PrP substrate (Hamster-sheep, FL Hu, and FL Hu E200K). The RT-QuIC reaction's signal-kinetic was measured and analyzed according to following semi-quantitative parameter, the duration of lag phase and AUC. In all the parameters of interest, no significant difference was observed between hamster-sheep, FL Hu and FL Hu E200K substrates in FFI CSF samples (Figure 18).

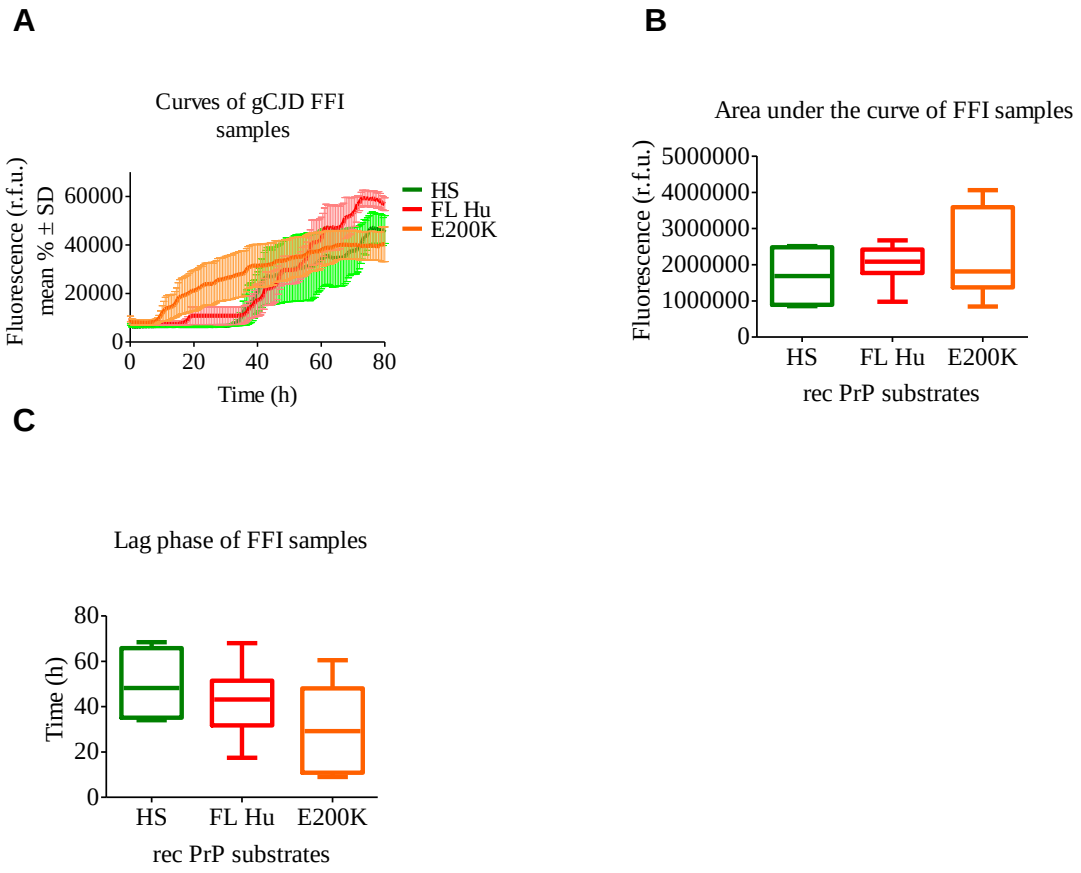

Figure 18. Influence of hamster-sheep, FL Hu, and FL Hu E200K substrates on the RT-QuIC signal response in FFI.

RT-QuIC reactions were seeded with CSF from non- CJD controls (n=44) and FFI samples (n=22). (A, B, C, D) FL Hu and FL Hu E200K substrates showed no significant difference in all RT-QuIC parameters used for a semi-quantitative analysis.

5.1 Determination of diagnostic accuracy of different substrates on the RT-QuIC assay in FFI samples

To investigate the diagnostic accuracy for FFI, we analyzed the RT-QuIC signal response of 22 FFI CSF samples running in triplicates for each substrate. We counted all patients with a positive signal response in at least two out of three RT-QuIC reactions as FFI positive. The sensitivity of the hamster-sheep substrate was 23 %, FL Hu substrate was 36 %, and FL Hu E200K substrate was 82 % for FFI samples (Table 15).

Table 15. Overview of diagnostic accuracy in FFI CSF samples.

The table recapitulates the RT-QuIC results in hamster-sheep, FL Hu, and FL Hu E200K in FFI CSF samples.

	Hamster-sheep	FL Hu	FL Hu E200K
FFI CJD	5/22 (23 %)	8/22 (36 %)	18/22 (82 %)
Non-CJD controls	0/44 (100 %)	0/44 (100 %)	0/44 (100 %)

6. Influence of different prion diseases on the RT-QuIC seeding response

To investigate the impact of different prion diseases on the RT-QuIC seeding response, we analyzed the signal kinetic from 20 sCJD, 15 gCJD E200K, and 8 FFI CJD RT-QuIC reactions in dependency from the kind of substrate. Hamster-sheep substrate revealed no significant difference in the AUC and lag phase between sCJD and gCJD E200K CSF samples (Figure 19, A2, A3). The RT-QuIC reaction applying FL Hu substrate shows no significant difference between all prion diseases groups (Figure 19, B2, B3). In the RT-QuIC reaction using FL Hu E200K substrate, we observed a significant shorter lag phase in E200K CSF samples when compared with sCJD (** $p \leq 0,01$) and FFI (* $p \leq 0,05$) samples but no significant difference between sCJD and FFI samples (Figure 18, C3). AUC is also significantly higher in gCJD E200K CSF samples when compared with sCJD (* $p \leq 0,05$) and FFI (* $p \leq 0,05$) CSF samples but no difference could be obtained between sCJD and FFI (Figure 19, C2).

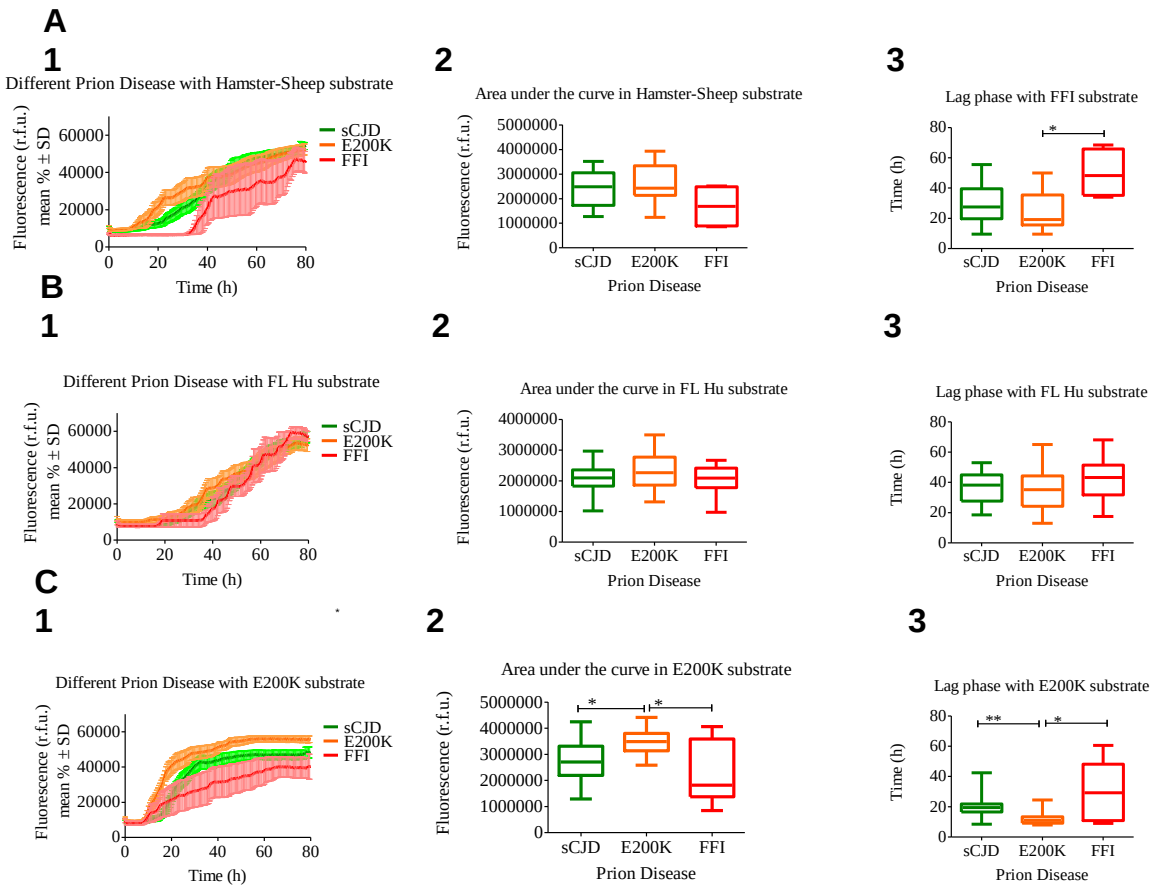

Figure 19. Influence of different prion diseases on the RT-QuIC Seeding Response in dependency from the kind of rec PrP substrate.

(A,1) Mean of fluorescence curves (+/- SD) of 20 sCJD (green curve), 15 gCJD E200K (orange curve) and 8 FFI CJD (red curve) fluorescent curves of the RT-QuIC reactions using hamster-sheep substrate. (A,2) AUC of the sCJD, gCJD E200K and FFI CSF samples using hamster-sheep as a substrate. (A,3) Lag phase of the sCJD, gCJD E200K and FFI CSF samples using hamster-sheep as a substrate. (B,1) Mean of the different prion diseases fluorescent curves (+/- SD) of the RT-QuIC reactions using FL Hu substrate. (B,2) Mean of AUC (+/- SD) of the different prion diseases groups using FL Hu as a substrate. (B,3) Lag phase of the different prion disease using FL Hu as a substrate. (C,1) Mean of the different prion diseases fluorescent curves (+/- SD) of the RT-QuIC reactions using FL Hu E200K substrate. (B,2) AUC of the different prion diseases groups using FL Hu E200K as a substrate. (B,3) Lag phase of the different prion disease using FL Hu E200K as a substrate.

7. Examination of the agreement between different rec PrP substrates in a prospective study

In a prospective study on a patient cohort of 134 CSF samples with unknown diagnoses, we performed RT-QuIC analysis applying different rec PrP substrates FL Hu and FL Hu E200K. As a reference, we used the routine diagnostic implemented hamster-sheep substrate [127,128]. To determine the analytical agreement among different rec PrP substrates, we examined the samples from the prospective cohort in parallel; CSF from the same patients were analyzed on the same plate with different rec PrP substrates.

Interestingly, we obtained an agreement between hamster-sheep and FL Hu of 86,56 % (Table 16) and between hamster-sheep and FL Hu E200K an agreement of 82,28 % (Table 17). In addition, we calculated Cohen's kappa value to determine the agreement between hamster-sheep and FL Hu, and between hamster-sheep and FL Hu E200K RT-QuIC results. We obtained a Cohen's value of 0,678, which indicates a substantial agreement (0,01 – 0,20 slight agreement, 0,21 – 0,40 fair agreement, 0,41 – 0,60 moderate agreement, 0,61 – 0,80 substantial agreement, 0,81 – 1,00 almost perfect or perfect agreement) between hamster-sheep and FL Hu RT-QuIC results. For the hamster-sheep and FL Hu E200K comparison, we calculated a Cohen's value of 0,628, which indicates a substantial agreement between both substrates.

Table 16. Agreement between hamster-sheep and FL Hu substrates in a prospective study.

We analyzed the agreement between hamster-sheep (standard substrate) and FL Hu in the RT-QuIC results. A positive RT-QuIC signal response was indicated by "+" and a negative one by "-".

	FL Hu RT-QuIC +	FL Hu RT-QuIC -	Agreement (%)	Kappa value
Hamster-sheep RT-QuIC +	**30**	**16**	**86,56%**	**0,678**
Hamster-sheep RT-QuIC -	**2**	**86**		

Table 17. Agreement between Hamster-sheep and FL Hu E200K substrates in a prospective study.

We analyzed the agreement between hamster-sheep (standard substrate) and FL Hu E200K in the RT-QuIC results.

A positive RT-QuIC signal response was indicated by "+" and a negative one by "-".

	FL Hu E200K RT-QuIC +	FL HU E200K RT-QuIC -	Agreement (%)	Kappa value
Hamster-sheep RT-QuIC+	**44**	**2**	**82,28%**	**0,628**
Hamster-sheep RT-QuIC-	**26**	**86**		

8. Competitive seeding induction of the different rec PrP substrates on the RT-QuIC

To investigate the interference that different rec PrP substrates could have during the RT-QuIC, different rec PrP substrates were mixed in equal parts and subjected to RT-QuIC analysis. For each group we run four sCJD and non-CJD CSF samples in triplicates together with two different substrates (mixed in equal parts) in the RT-QuIC reaction. We investigated following substrate combinations: i) hamster-sheep mixed with FL Hu, ii) hamster-sheep mixed with FL Hu E200K, and iii) FL Hu mixed with E200K) (Figure 20, A1, B1, C1). RT-QuIC seeding response with hamster-sheep mixed with FL Hu showed a significant shorter lag phase when compared with FL Hu substrate (* $p \leq 0,05$) but no significant difference when compared with hamster-sheep substrate (Figure 20, A3). Regarding the AUC values the combination of hamster-sheep mixed with FL Hu substrate indicated no significant difference when compared with FL Hu and hamster-sheep substrate (Figure 20, A2). hamster-sheep mixed with FL Hu E200K substrate revealed a significantly longer lag phase when compared with FL Hu E200K substrate (** $p \leq 0,01$) but no significant difference when compared with hamster-sheep substrate (Figure 20, B3). AUC values of the hamster-sheep mixed with FL Hu E200K substrate comparison were significantly different in compare with FL Hu E200K (** $p \leq 0,01$) but no significant difference when compared with hamster-sheep substrate (Figure 20, B2). FL Hu mixed with FL Hu E200K substrate showed a significantly longer lag phase in comparison with FL Hu E200K (* $p \leq 0,05$) but no significance when compared with FL Hu (Figure 20, C3).

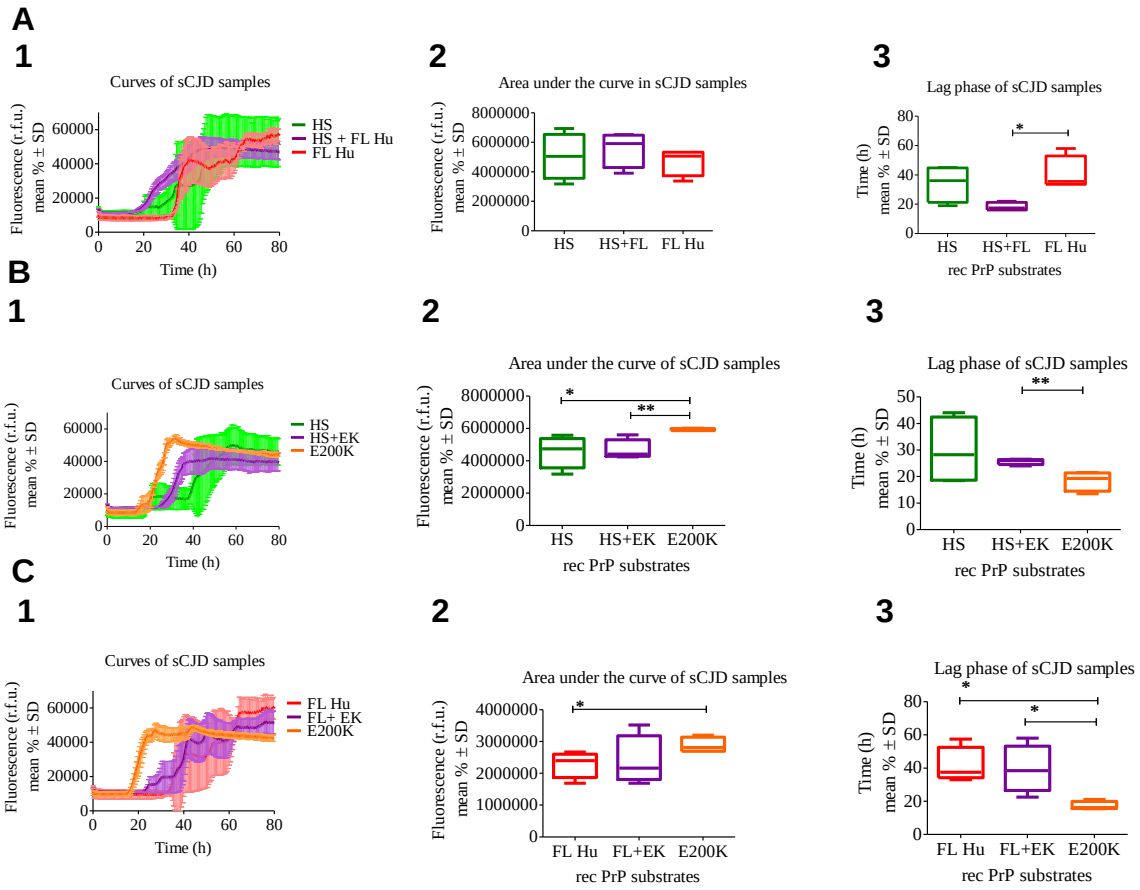

Figure 20. Competitive seeding induction of different rec PrP substrates in the RT-QuIC.

(A1) Mean of fluorescence curves (+/- SD) of RT-QuIC reactions seeded with four sCJD samples with hamster-sheep substrate (green curve), Hamster-sheep mixed with FL Hu substrate (violet curve) and FL Hu substrate (red curve). (B1) Mean of fluorescence curves (+/- SD) of RT-QuIC reactions seeded with four sCJD samples with hamster-sheep substrate (green curve), hamster-sheep mixed with FL Hu E200K (EK) substrate (violet curve) and FL Hu E200K substrate (orange curve). (C1) Mean of fluorescence curve (+/- SD) of the RT-QuIC reactions seeded with four sCJD samples with FL Hu substrate (red curve), FL Hu mixed with FL Hu E200K (EK) substrate (violet curve) and FL Hu E200K substrate (orange curve). (A2,B2,C2) AUC of the RT-QuIC seeding response with different rec PrP substrates . (A3,B3,C3) Lag phase of the RT-QuIC seeding response with different rec PrP substrates.

9. Transmission electron microscopy

To investigate the structural features of the RT-QuIC product aggregates from different prion diseases with different rec. PrP substrates, we analyzed the RT-QuIC product by using transmission electron microscopy (TEM) analyses.

In the RT-QuIC product seeded with sCJD (MM) CSF samples (Figure 21, line A), TEM analysis showed the generation of a PrP^{Res} fibrils during the RT-QuIC assay using hamster-sheep rec PrP as a substrate (Figure 21, A1). TEM investigation of RT-QuIC products using FL Hu rec PrP substrate (Figure 21, A2) revealed the presence of abundant PrP^{Res} fibrils; the density of the fibrils even increased when using FL Hu E200K substrate for amplification (Figure 21, A3).

In the RT-QuIC product seeded with gCJD E200K CSF samples (Figure 21, line B), TEM examinations revealed the generation of PrP^{Res} fibrils when used hamster-sheep as a substrate (Figure 21, B1). Samples from the RT-QuIC product using FL Hu substrate (Figure 21, B2) showed the presence of few-moderate fibrils in the sample, as well when using FL Hu E200K as a substrate (Figure 21, B3).

In the RT-QuIC product seeded with FFI CJD CSF samples (Figure 21, line C), TEM analysis showed the presence of a moderate number of fibrils when used hamster-sheep as a substrate (Figure 20, C1). Samples from the RT-QuIC product using FL Hu (Figure 21, C2) and FL Hu E200K (Figure 21, C3) substrate showed the presence of abundant fibrils in the samples.

All the RT-QuIC products seeded with non-CJD CSF samples using hamster-sheep (Figure 21, D1), FL Hu (Figure 21, D2), and FL Hu E200K (Figure 21, D3) showed no formation of PrP^{Res} fibrils; some amorphous artifacts were visible (Figure 21, D2).

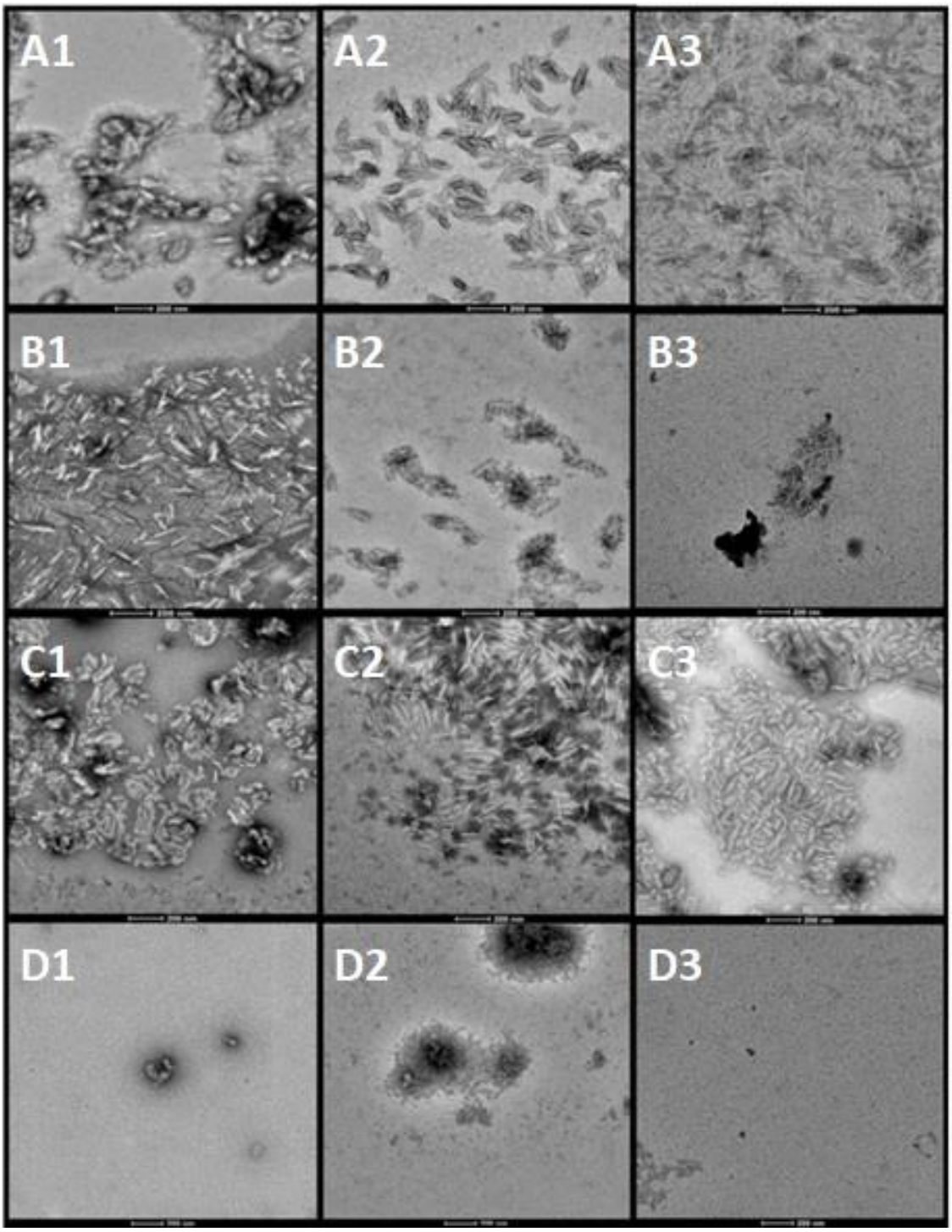

Figure 21. Transmission electron microscopy images of RT-QuIC product.

Transmission electron microscopy images of RT-QuIC product (scale bar = 200nm) when using hamster-sheep as a substrate and sCJD CSF as a seed (A1), gCJD E200K CSF as a seed (B1), FFI CJD as a seed (C1), and non-CJD controls (D1). RT-QuIC product when using FL-Hu as a substrate and sCJD CSF as a seed (A2), gCJD E200K CSF as a seed (B2), FFI CJD as a seed (C2), and non-CJD controls (D2). RT-QuIC

product when using FL Hu E200K mutation as a substrate and sCJD CSF as a seed (A3), gCJD E200K CSF as a seed (B3), FFI CJD as a seed (C3), and non-CJD controls (D3).

10. Detection of PrP^{Sc} in prion disease tear fluid samples via RT-QuIC applying FL Hu E200K substrate

To explore for the first time the PrP^{Sc} amplification detection in prion disease tear fluid samples applying the most sensitive rec PrP FL Hu E200K substrate, 20 prion disease and 16 non-prion disease control samples were subjected to RT-QuIC analysis using the standard protocol [86] with a modification of 130 h instead of 80 h running. Each patient sample was run in triplicates, and it was considered as positive for prion disease when at least two out of three replicates showed a positive signal response. All controls were tested negative and 13 out of 20 prion disease samples were considered as positive. The quantification of the signal RT-QuIC signal response occurred by following three parameters of interest: lag phase, AUC, and the maximum signal of RT-QuIC response (Figure 22).

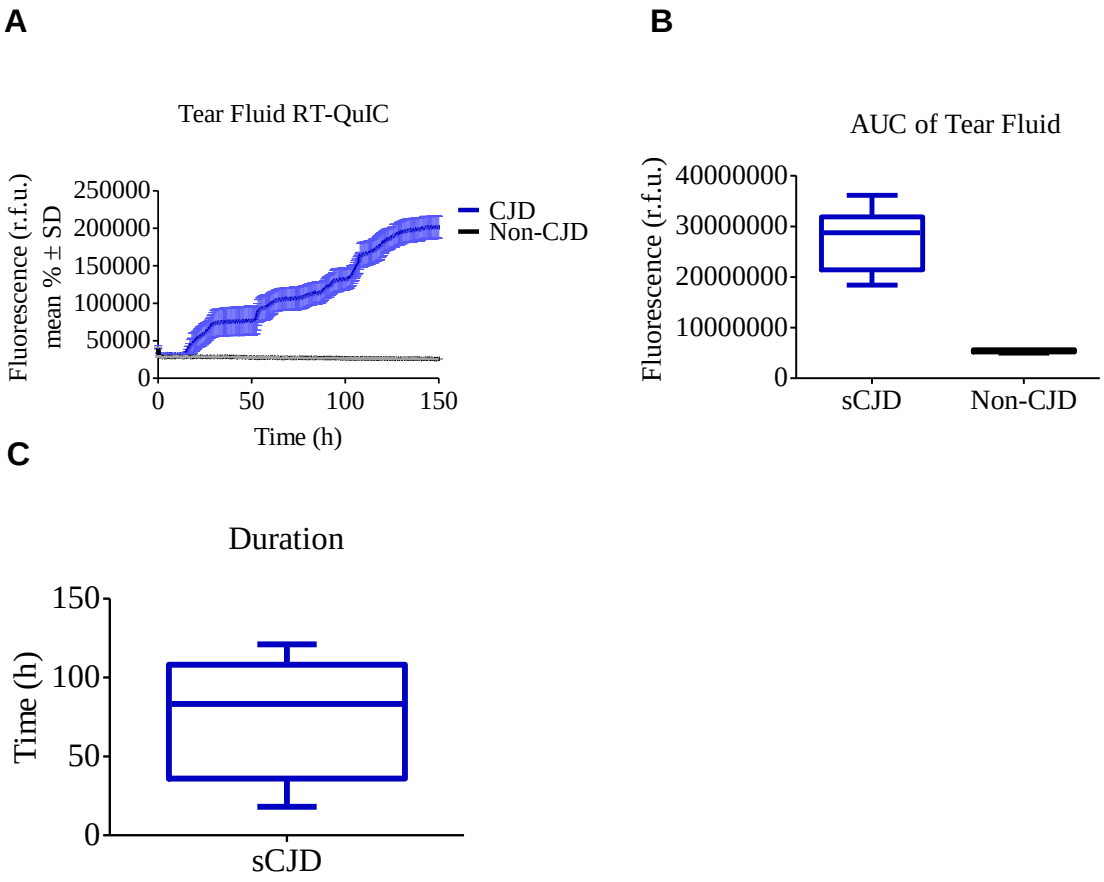

Figure 22. Influence of FL Hu E200K substrate on the RT-QuIC signal response in prion disease tear fluid samples.

(A) Mean of the positive curves (+/- SD) seed with prion disease tear fluid samples (n=8) and mean of non-CJD controls (n=6) samples (n=8). (B) AUC. (C) Lag phase.

10.1 Diagnostic accuracy of the tear fluid in the RT-QuIC assay

To investigate the diagnostic accuracy in prion disease tear fluid samples, we analyzed the RT-QuIC signal response of 20 prion disease and 16 non-prion disease samples running in triplicates. We counted all samples with at least two of the three positive RT-QuIC reactions as positive for prion disease. Interestingly, the sensitivity of the prion disease tear fluid was 75 % and specificity of 100 % (Table 18).

Table 18. Overview of diagnostic accuracy in prion disease tear fluid Samples.

The table recapitulates the RT-QuIC results in FL Hu E200K substrate from prion disease tear fluid samples.

	FL Hu E200K
CJD tear fluid	18/24 (75%)
Non-CJD controls tear fluid	16/16 (100%)

10.2 Examination of the accuracy and agreement between CSF and tear fluid RT-QuIC

To examine the agreement between CSF and tear fluid RT-QuIC in prion diseases, we analyzed 25 samples from non-prion disease and prion disease patients. The obtained agreement was 84 % between CSF and tear fluid RT-QuIC results (Table 19). In addition, we calculated Cohen's kappa value to determine the agreement between the CSF and tear fluid RT-QuIC. We obtained a Cohen's value of 0,615, which indicates substantial agreement between the two RT-QuIC assays.

Table 19. Agreement between CSF and tear fluid RT-QuIC.

A positive RT-QuIC signal response was indicated by "+" and a negative one by "-".

	Tear fluid RT-QuIC +	**Tear fluid RT-QuIC -**	**Agreement (%)**	**Cohen's Kappa value**
CSF RT-QuIC +	5	4	84%	0,615
CSF RT-QuIC -	0	16		

VI. Discussion

Standard *post-mortem* neuropathological techniques such as immunoassays allowed the detection of PrP^{Sc} in human tissues with high infection levels of prions, such as lymphoid and brain tissue. Although, in most accessible *pre-mortem* diagnostic specimens, such as blood, CSF, and tear fluid, these techniques cannot detect prion infectivity due to the low infection levels of PrP^{Sc} in these specimens [129].

In contrast, *in vitro* protein misfolding conversion assays, such as the PMCA or RT-QuIC, techniques based on the PrP^{Sc} ability to induce a misfolding conversion of PrP^{C}, can amplify minuscule amounts of PrP^{Sc}, present in the low infectivity specimens to a detectable level, e.g., in CSF. Currently these methods are widely used for routine diagnosis of prion disease. However, the RT-QuIC assay has not yet been standardized among different reference laboratories who apply different kinds of rec PrP substrates and different protocols.

In the present study, we studied the seeding conversion efficiency of different rec PrP substrates in sCJD and the most common genetic prion diseases, such as gCJD E200K, and FFI. Our aim is to identify an universal rec PrP substrate for the RT-QuIC assay to diagnose different kinds of prion diseases with a high diagnostic accuracy.

We hypothesize that rec PrP substrates with with prion disease mutations in the RT-QuIC may facilitate the conversion of PrP^{C} into PrP^{Sc} [130,131].

1. RT-QuIC reaction applying different rec PrP substrates is resistant to defined storage conditions

The key feature in the RT-QuIC reaction is the selection of a rec PrP substrate capable of detecting low levels of PrP^{Sc} in prion disease samples. Additionally, the substrate needs to be stable along the constant cycles of shaking and should not show self-aggregation properties in the RT-QuIC reactions seeded with non-CJD control samples [86]. Familial prion disease mutations, such as E200K and FFI, are known to lead to a structural alteration of the cellular PrP that promotes the spontaneous conformal change of PrP^{C} into PrP^{Sc} [130,131]. Introducing these familial prion disease mutations in a rec PrP substrate for the RT-QuIC may increase the self-aggregation properties of the substrates which needs to be ruled out when used for futher analysis.

A further problem may occur with research samples from a biobank that undergo numerous freezing and thawing cycles, which may have an influence on the stability of diagnostic marker. We aimed to explore the possibility that the rec PrP may spontaneously self-agggregate without misfolded seed and, consequently, give a false positive reaction in the RT-QuIC or the possibility that numerous freezing and thawing cycles of the CJD samples could decrease the signal response of the RT-QuIC reaction. Thus, we ran the RT-QuIC with CJD samples subjected to up to twelve cycles of freezing and thawing, non-CJD samples, non-CJD samples without substrate, and only with the rec PrP substrate. RT-QuIC reactions without CSF and non-CJD samples produced no positive RT-QuIC signal when using hamster-sheep, FL Hu, and FL Hu E200K substrates.

In contrast, we observed that the rec PrP substrate with FFI mutation produced a false positive signal response in the RT-QuIC reactions seeded with non-CJD CSF control as well as without addition of CSF.

In summary, our findings ruled out the possibility of self-aggregation when when using hamster-sheep, FL Hu, and FL Hu E200K rec PrP as substrates in the RT-QuIC. However, the FL Hu FFI substrate, which was prone to self-aggregation, was excluded from further analysis.

In addition, we could prove that different rec PrP substrates, applied in in the RT-QuIC reactions with sCJD CSF samples, were resistant to 12 repeated freezing and thawing cycles. In addition, the quantitative parameter of the signal response curve were not significantly changed by 12 repeated freezing and thawing cycles. Our obtained data, were in line with a previous study, where sCJD CSF samples were subjected to twelve cycles of freezing and thawing cycles without significant changes in the signal response curves[82]. FL Hu and FL Hu E200K substrates were therefore considered for further analysis.

2. Comparison of the seeding conversion efficiencies and diagnostic accuracies of rec hamster-sheep, FL HU, and FL Hu E200K PrP substrates

Improved *pre-mortem* diagnostic testing for prion disease have a significant value in medical and public health system. A rapid and accurate diagnosis is fundamental

important for therapeutic interventions in future, for the exlclusion of a prion disease or to prevent iatrogenic infections [132]. [133,134].

In order to identify the most suitable rec PrP substrate for RT-QuIC assay, with a short analytical time and an universal application, also for FFI, we have put together a study cohort, consisting of CSF from sCJD, gCJD (E200K), FFI and non-prion disease samples. In the RT-QuIC reaction we analysed the seeding conversion efficiency and the diagnostic accuracy of different rec PrP substrates (hamster-sheep, FL Hu, and FL Hu E200K).

Our data indicated that the rec PrP FL Hu E200K substrate significantly increases the seeding conversion reaction of PrP in compared with the FL Hu substrate without mutation and hamster-sheep substrate. Moreover, the study suggests that the rec PrP FL Hu E200K substrate reduced the duration of the lag phases. Consequently, it can be considered to reduce the duration of the RT-QuIC assay from currently 80 h.

In contrast to the Hu E200K substrate, the hamster-sheep substrate needed more than 11 h, and the FL Hu substrate more than 13 h longer assay time to detect 98 % of the prion positive samples.

Other studies on CSF RT-QuIC using FL rec PrP substrates (mostly with the hamster *PRNP* sequence) also followed a protocol with a total assay duration of 80 to 90 h. However, studies using truncated hamster substrate with the addition of SDS show a reduction of the assay of 80 h to 60 h time (Table 22) [135–139]. A similar reduction might be considered when applying FL Hu E200K substrate in the RT-QuIC.

Another advantage of using FL Hu E200K substrate beside a shorter assay duration is the elevated sensitivity and specificity, up to 95 % and 100 % respectively, without adding SDS in the reaction buffer and increasing the temperature to 55 ^{o}C (instead of 42 ^{o}C).

Subsequently, we examined the seeding conversion efficiency of different rec PrP substrates in three different *PRNP* codon 129 MV sCJD genotypes. Again, FL Hu E200K substrate demonstrated the highest sensitivity to detect all sCJD genotypes, reaching 100 % sensitivity in sCJD MV and VV genotypes. When we analyzed the sensitivity of FL Hu E200K substrate in different sCJD subtypes, we observed a 100% sensitivity for sCJD

VV2 subtype and for the atypical and rare MV2K type. A sensitivity below 100 % was obtained in the MM1/MV1 subtype and the MM genotype, 92 % and 79 %, respectively. Even the lowest sensitivity in the MM genotype obtained using FL Hu E200K is higher than the sensitivities observed from hamster-sheep and FL Hu substrates. Compared to other studies FL Hu E200K substrate revealed an equal sensitivity for the sCJD codon 129 MM genotype and sCJD MM1/MV1 (Table 23, 24). subtype. In our hands, FL Hu E200K substrate was the most accurate and universal substrate, able to diagnose different sCJD subtypes with a good diagnostic accuracy.

Additionally, the FL Hu E200K substrate demonstrated high sensitivity in both genetic prion disease cases, 100 % in E200K and 82 % in FFI cases, contrary to the FL Hu and hamster-sheep, which showed poor sensitivity of 23 % and 36 %, respectively, in FFI samples. Our data from hamster-sheep and FL Hu align with four previous studies, which reported low sensitivity between 16.2 % and 57 % of the RT-QuIC for FFI cases [127,140–142]. Only one study using a FL Hu substrate reported a sensitivity of 83.3% for FFI cases, which differs from our obtained the sensitivity of 36 % for FFI cases. [143]. This discrepancy may be explained by the composition and the number of FFI cases in the cohort, differences in the RT-QuIC protocol as well in the protocol for substrate production and purification. Overall, this study showed a high accuracy of the FL Hu E200K substrate in CJD and FFI.

Table 20. Overview of diagnostic accuracy in RT-QuIC.

Sensitivity and specificity of sCJD CSF RT-QuIC in different studies and sensitivity in genetic prion diseases CSF samples in the RT-QuIC.

Species	Amino acid	Accuracy for sCJD CSF Sensitivity/Specificity		CSF gCJD E200K	CSF FFI	References
Human	23-231	80% (27/34)	100% (0/49)	82% (18/22)	83% (10/12)	Atarashi *et al* [144] Sano *et al* [143]
Hamster	23-231	89% (109/123) 88.2% (148/179)	99% (1/103) 99.4% (1/163)	62.5% (10/16)	16.7% (4/24)	McGuire *et al* [79] Lattanzio *et al*. [145] Kang Xiao *et al* [140]
	90-231	94% (106/113) 92% (102/111) 95% (60/63) 95% (58/61)	100% (0/64) 98.5% (1/67) 100% (14/14) 100% (0/80)	44.0% (11/25)	16.2% (6/37)	Groveman *et al* [135] Foutz *et al* [138] Foutz *et al* [146] Fiorini *et al* [147] HU Chao *et al* [141]
Bank vole 23-230		88.6% (70/79)	91.2% (5/57)	100% (3/3)	50% (1/2)	Mok TH *et al* [142]
Hamster-sheep chimera	Hamster 23-137 Sheep 141-234	80% (51/64) 89% (163/183)	99% (2/400) 100% (0/118)	100 % (33/33)	57% (4/7)	Cramm *et al* [127] Hermann *et al* [76]

Table 21. Overview of diagnostic accuracy in sCJD CSF RT-QuIC in different *PRNP* codon 129 M/V genotypes.

		Sensitivity in different sCJD genotypes			
Species	**Patients (n)**	**MM**	**MV**	**VV**	**References**
FL Human	34	86 %	100 %	75 %	Atarashi *et al* [144]
FL Hamster	89 87 69 83	90 % 78 % 71 % 84 %	88 % 75 % 66 % 72 %	95 % 100 % 33 % 80 %	McGuire *et al* [79] Orru *et al* [148] Groveman *et al* [135] Lattanyio *et al* [149]
Truncated Hamster	96 94 92 93	95 % 94 % 92 % 94 %	100 % 66 % 92 % 94 %	100 % 66 % 98 % 94 %	Orru et al [150] Groveman *et al* [151] Franceschini *et al* [152] Foutz *et al* [153]

Table 22. Overview of diagnostic accuracy of the RT-QuIC in different sCJD subtypes.

Species	Patients (n)	MM/MV1	VV2	MV2K	References
FL Hamster	111 27 81	89 %	78 %	26 %	Alison J E Green [154]
Truncated Hamster	119 27 9	96 %	100 %	89 %	Alison J E Green [154]
	43 33 26	93 %	100 %	92.3%	Franceschini *et al* [152]

3. Optimization of RT-QuIC assay for the detection of PrP^{Sc} in tear fluids

Lumbar puncture for the collection of CSF is a well-established and commonly applied in diagnosis of neurodegenerative diseases, e.g. for the measurement of specific biomarkers. [155–157]. Despite its widespread use, there are several drawbacks. For example, lumbar punctures are invasive for the patients. They additionally require expertise of a physician and are relatively time-consuming.

In prion disease diagnostic several studies have been undertaken to detect PrP^{Sc} in a less invasive biological fluid without losing the high accuracy of the CSF RT-QuIC. Studies using peripheral tissue homogenates from olfactory mucosa and skin have shown high sensitivity, 97 % and 95,5 % respectively, in detecting PrP^{Sc} in patients with prion disease [158–160]. Although collecting skin and olfactory mucosa tissue samples requires punch biopsy and nasal brushing, these techniques are still invasive. A study using *post mortem* ocular tissues demonstrated the presence of the PrP^{Sc} infection in the eye of CJD cases [161], supporting the idea of the transmission of the PrP^{Sc} through the connection between the efferent nerves originating in the CNS and the lacrimal gland (Figure 23) [162]. Based on that, we hypothesized that using a sensitive rec PrP substrate (e.g., FL Hu E200K) in the RT-QuIC may allow the detection of PrP^{Sc} via RT-QuIC, seeded with less-invasive biological fluid such as tear fluid from prion disease patients.

In our study, we subjected a set of tear fluid samples derived from CJD patients and non-CJD patients using rec PrP FL Hu E200K substrate to RT-QuIC analysis.

Interestingly, our data showed for the first time that using rec PrP FL Hu E200K substrate in the RT-QuIC enable the detection of PrP^{Sc} in tear fluid samples from CJD patients.

The RT-QuIC analysis of 24 CJD patients revealed a good sensitivity of 75 %, while the specificity remained at 100 %. Compared to the CSF RT-QuIC using hamster-sheep substrate [88], the sensitivity is approximately 5-10 % lower while specificity of the tear fluid RT-QuIC was similar, however the sample size was lower, suggesting that the promising results of our current study needs to be confirmed in a higher number of well-

characterized samples, as well as in different patient cohorts. To prove the reproducibility of the tear fluid RT-QuIC, ring trial studies employing different reference laboratories are planned.

Altogether, our study demonstrated that rec FL Hu E200K substrate can be used as substrate for the RT-QuIC to diagnose CJD applying less-invasive tear fluid samples. The new tests opens new avenues for the analysis pre-clinical patient samples and/or follow-up studies in future to evaluate the efficiency of therapeutic intervention.

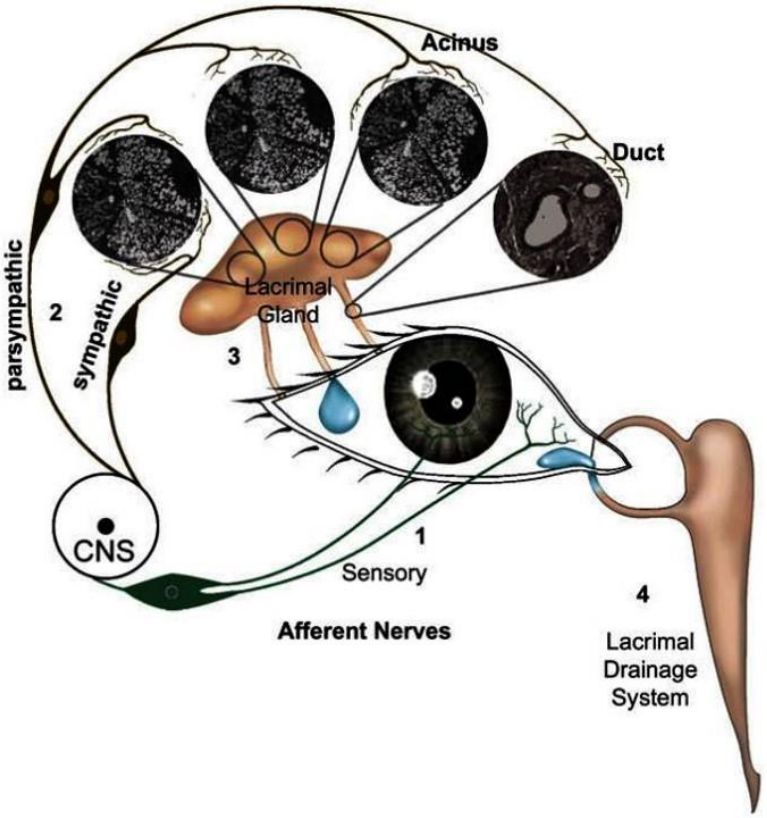

Figure 23. Lacrimal gland functional unit.

Activation of the afferent nerves (1) project through central nervous system (CNS) to stimulate efferent parasympathetic and sympathetic nerves (2) that innervate the lacrimal gland (3) and induce secretion of lacrimal gland fluid onto the ocular surface that drains into the lacrimal drainage system (4). Figure taken from Dartt (2009) [163].

VII. Summary and Conclusion

Prion diseases are fatal neurological disorders. For routine CSF diagnostics, in vitro protein misfolding amplification assays, such as RT-QuIC, had already been established. This assay applies a rec PrP substrate, which becomes converted by a PrP^{Sc} seed derived either from tissue or biological fluid of prion disease patients. Currently, the CSF RT-QuIC has a sensitivity of 80-89 %, and the specificity is 99-100 % for sCJD diagnosis. However, the sensitivity of the RT-QuIC to diagnose FFI cases is very low (approximately 30%).

In the present study, we aimed to identify the most suitable rec PrP substrate for RT-QuIC assay, with short assay duration and universal application for different prion diseases, such as FFI, and to detect PrP^{Sc} in less invasive body fluids. Based on these aims, we performed CSF RT-QuIC analysis applying rec PrP substrates with PRNP sequences from different species (hamster-sheep, FL Hu, FL Hu E200K, and FL Hu FFI) in different prion diseases (sCJD, gCJD E200K and FFI).

In a retrospective study, we showed that rec PrP FL Hu with E200K was observed to be the most efficient and accurate substrate in the CSF RT-QuIC for prion disease diagnosis.

Interestingly, the rec PrP FL Hu E200K substrate increased the sensitivity for sCJD patients (different PRNP codon 129 MV geno- and subtypes) up to 95 % and in the most common genetic prion diseases, e.g., E200K to 100 % and FFI to 82 %.

Transmission electron microscopy analysis indicated the formation of PrP fibrils during the RT-QuIC exhibiting subtle morphological appearances. A mixture of different rec PrP substrates (e.g., Hu E200K substrate with hamster-sheep) provoked a mean signal response in the RT-QuIC, which indicates that two rec PrP substrates with different PRNP sequences do not inhibit each other; they were able to convert and aggregate independently from each other.

Finally, we demonstrated that FL Hu E200K substrate enables the detection of PrP^{Sc} in tear fluid samples from prion disease patients, with a good sensitivity of 75 %, suggesting FL Hu E200K as a universal substrate for the prion disease diagnostic via RT-QuIC. Moreover, it enables the detection of PrP^{Sc} in less-invasive body fluids, which may be quite useful for diagnostic and follow-up studies, e.g., after therapeutic intervention.

VIII. Bibliography

1. Acevedo-Morantes, C. Y. & Wille, H. The structure of human prions: From biology to structural models — considerations and pitfalls. *Viruses* vol. 6 3875–3892 Preprint at https://doi.org/10.3390/v6103875 (2014).

2. Carleton, A., Tremblay, P., Vincent, J. D. & Lledo, P. M. Dose-dependent, prion protein (PrP)-mediated facilitation of excitatory synaptic transmission in the mouse hippocampus. *Pflugers Arch* **442**, 223–229 (2001).

3. Colling, S. B., Collinge, J. & Jefferys, J. G. R. *H[gROSCIgiC[STillS Hippocampal slices from prion protein null mice: disrupted Ca2*-activated K ÷ currents*. *Neuroscience Letters* vol. 209 (1996).

4. Criado, J. R. *et al.* Mice devoid of prion protein have cognitive deficits that are rescued by reconstitution of PrP in neurons. *Neurobiol Dis* **19**, 255–265 (2005).

5. Coitinho, A. S., Roesler, R., Martins, V. R., Brentani, R. R. & Izquierdo, I. Cellular prion protein ablation impairs behavior as a function of age. *Neuroreport* **14**, 1375–1379 (2003).

6. Roguski, A. & Gill, A. C. pathogens The Role of the Mammalian Prion Protein in the Control of Sleep. (2017) doi:10.3390/pathogens6040058.

7. Mercer, R. C. C. *et al.* The prion protein modulates A-type K+ currents mediated by Kv4.2 complexes through dipeptidyl aminopeptidase-like protein 6. *Journal of Biological Chemistry* **288**, 37241–37255 (2013).

8. Herms, J. W. *et al. Altered Intracellular Calcium Homeostasis in Cerebellar Granule Cells of Prion Protein-Deficient Mice*. *J. Neurochem* vol. 75 (2000).

9. Fuhrmann, M. *et al.* Loss of the cellular prion protein affects the Ca2+ homeostasis in hippocampal CA1 neurons. *J Neurochem* **98**, 1876–1885 (2006).

10. Powell, A. D., Toescu, E. C., Collinge, J. & Jefferys, J. G. R. Alterations in Ca2+-buffering in prion-null mice: Association with reduced afterhyperpolarizations in CA1 hippocampal neurons. *Journal of Neuroscience* **28**, 3877–3886 (2008).

11. Carulla, P. *et al.* Neuroprotective role of PrP c against kainate-induced epileptic seizures and cell death depends on the modulation of JNK3 activation by GluR6/7-PSD-95 binding. *Mol Biol Cell* **22**, 3041–3054 (2011).

12. Khosravani, H. *et al.* Prion protein attenuates excitotoxicity by inhibiting NMDA receptors. *Journal of Cell Biology* **181**, 551–555 (2008).

13. Gadotti, V. M. & Zamponi, G. W. Cellular prion protein protects from inflammatory and neuropathic pain. *Mol Pain* **7**, (2011).

14. Gadotti, V. M., Bonfield, S. P. & Zamponi, G. W. Depressive-like behaviour of mice lacking cellular prion protein. *Behavioural Brain Research* **227**, 319–323 (2012).

15. Beraldo, F. H. *et al.* Role of α7 nicotinic acetylcholine receptor in calcium signaling induced by prion protein interaction with stress-inducible protein. *Journal of Biological Chemistry* **285**, 36542–36550 (2010).

16. Prestori, F. *et al.* Altered neuron excitability and synaptic plasticity in the cerebellar granular layer of juvenile prion protein knock-out mice with impaired motor control. *Journal of Neuroscience* **28**, 7091–7103 (2008).

17. Laurén, J., Gimbel, D. A., Nygaard, H. B., Gilbert, J. W. & Strittmatter, S. M. Cellular prion protein mediates impairment of synaptic plasticity by amyloid-B oligomers. *Nature* **457**, 1128–1132 (2009).

18. Weise, J. *et al.* Deletion of cellular prion protein results in reduced Akt activation, enhanced postischemic caspase-3 activation, and exacerbation of ischemic brain injury. *Stroke* **37**, 1296–1300 (2006).

19. Mitteregger, G. *et al.* The role of the octarepeat region in neuroprotective function of the cellular prion protein. *Brain Pathology* **17**, 174–183 (2007).

20. Doeppner, T. R. *et al.* Cellular prion protein promotes post-ischemic neuronal survival, angioneurogenesis and enhances neural progenitor cell homing via proteasome inhibition. *Cell Death Dis* **6**, e2024 (2015).

21. Brown, D. R., Schulz-Schaeffer, W. J., Schmidt, B. & Kretzschmar, H. A. *Prion Protein-Deficient Cells Show Altered Response to Oxidative Stress Due to Decreased SOD-1 Activity*. (1997).

22. Kleene, R. *et al.* Prion protein regulates glutamate-dependent lactate transport of astrocytes. *Journal of Neuroscience* **27**, 12331–12340 (2007).

23. Watt, N. T. *et al.* Prion protein facilitates uptake of zinc into neuronal cells. *Nat Commun* **3**, (2012).

24. Gasperini, L., Meneghetti, E., Legname, G. & Benetti, F. In absence of the cellular prion protein, alterations in copper metabolism and copper-dependent oxidase activity affect iron distribution. *Front Neurosci* **10**, (2016).

25. Br ief Definitive Repor t. (2016) doi:10.1084/jem.20151610.

26. Bremer, J. *et al.* Axonal prion protein is required for peripheral myelin maintenance. *Nat Neurosci* **13**, 310–318 (2010).

27. Thom, T. *et al.* Cellular Prion Protein Mediates α-Synuclein Uptake, Localization, and Toxicity In Vitro and In Vivo. *Movement Disorders* **37**, 39–51 (2022).

28. Resenberger, U. K. *et al.* The cellular prion protein mediates neurotoxic signalling of Î 2-sheet-rich conformers independent of prion replication. *EMBO Journal* **30**, 2057–2070 (2011).

29. Nicolas, O., Gavín, R. & del Río, J. A. New insights into cellular prion protein (PrPc) functions: The 'ying and yang' of a relevant protein. *Brain Research Reviews* vol. 61 170–184 Preprint at https://doi.org/10.1016/j.brainresrev.2009.06.002 (2009).

30. Harris, D. A. Trafficking, turnover and membrane topology of PrP. doi:10.1093/bmb/dg66.071.

31. Watts, J. C., Bourkas, M. E. C. & Arshad, H. The function of the cellular prion protein in health and disease. *Acta Neuropathologica* vol. 135 159–178 Preprint at https://doi.org/10.1007/s00401-017-1790-y (2018).

32. Prusiner, S.B., 2004. Detecting mad cow disease. Scientific American, 291(1), pp.86–93.

33. Novakofski, J., Brewer, M. S., Mateus-Pinilla, N., Killefer, J. & McCusker, R. H. Prion biology relevant to bovine spongiform encephalopathy. *Journal of Animal Science* vol. 83 1455–1476 Preprint at https://doi.org/10.2527/2005.8361455x (2005).

34. Moore, R. A., Taubner, L. M. & Priola, S. A. Prion protein misfolding and disease. *Current Opinion in Structural Biology* vol. 19 14–22 Preprint at https://doi.org/10.1016/j.sbi.2008.12.007 (2009).

35. Lee, J., Kim, S. Y., Hwang, K. J., Ju, Y. R. & Woo, H. J. Prion Diseases as Transmissible Zoonotic Diseases. *Osong Public Health and Research Perspectives* vol. 4 57–66 Preprint at https://doi.org/10.1016/j.phrp.2012.12.008 (2013).

36. Araújo, A. Q. C. Prionic diseases. *Arquivos de Neuro-Psiquiatria* vol. 71 731–737 Preprint at https://doi.org/10.1590/0004-282X201301461 (2013).

37. Burrell, C. J., Howard, C. R. & Murphy, F. A. *Fenner and White's Medical Virology: Fifth Edition*. *Fenner and White's Medical Virology: Fifth Edition* (Elsevier Inc., 2016).

38. Belay, E. D. *TRANSMISSIBLE SPONGIFORM ENCEPHALOPATHIES IN HUMANS*. www.annualreviews.org (1999).

39. Liemann, S. & Glockshuber, R. *BREAKTHROUGHS AND VIEWS Transmissible Spongiform Encephalopathies*. (1998).

40. Puoti, G. *et al.* Sporadic human prion diseases: molecular insights and diagnosis. *Lancet Neurol* **11**, 618–628 (2012).

41. Takeuchi, A. *et al.* Two distinct prions in fatal familial insomnia and its sporadic form. *Brain Commun* **1**, (2019).

42. Sitammagari, K. K. & Masood, W. Creutzfeldt Jakob Disease. *Enfermedad de Creutzfeldt-Jakob* (2022).

43. Salehi, P., Clark, M., Pinzon, J. & Patil, A. Sporadic Creutzfeldt-Jakob disease. *Am J Emerg Med* **52**, 267.e1-267.e3 (2022).

44. Sikorska, B., Knight, R., Ironside, J. W. & Liberski, P. P. Creutzfeldt-Jakob disease. *Adv Exp Med Biol* **724**, 76–90 (2012).

45. Lloyd, S. E., Mead, S. & Collinge, J. Genetics of prion diseases. *Curr Opin Genet Dev* **23**, 345 (2013).

46. Kobayashi, A., Kitamoto, T. & Mizusawa, H. Iatrogenic Creutzfeldt-Jakob disease. *Handb Clin Neurol* **153**, 207–218 (2018).

47. Masters, C. L. *et al. Creutzfeldt-Jakob Disease: Patterns of Worldwide Occurrence and the Significance of Familial and Sporadic Clustering*.

48. Ladogana, A. *et al. High incidence of genetic human transmissible spongiform encephalopathies in Italy*. (2005).

49. de Villemeur, T. B. Creutzfeldt-Jakob disease. in *Handbook of Clinical Neurology* vol. 112 1191–1193 (Elsevier B.V., 2013).

50. Parchi, P. *et al. Classification of Sporadic Creutzfeldt-Jakob Disease Based on Molecular and Phenotypic Analysis of 300 Subjects*. (1999).

51. Cali, I. *et al.* Co-existence of scrapie prion protein types 1 and 2 in sporadic Creutzfeldt-Jakob disease: Its effect on the phenotype and prion-type characteristics. *Brain* **132**, 2643–2658 (2009).

52. Puoti, G. *et al.* Sporadic human prion diseases: Molecular insights and diagnosis. *The Lancet Neurology* vol. 11 618–628 Preprint at https://doi.org/10.1016/S1474-4422(12)70063-7 (2012).

53. Safar, J. G. *et al. Sporadic human prion diseases: molecular insights and diagnosis*. *Review Lancet Neurol* vol. 11 www.thelancet.com/neurology (2012).

54. Karamujić-Čomić, H. *et al.* Prion protein codon 129 polymorphism in mild cognitive impairment and dementia: the Rotterdam Study. *Brain Commun* **2**, (2020).

55. Takada, L. T. & Geschwind, M. D. Prion diseases. *Semin Neurol* **33**, 348–356 (2013).

56. Gambetti, P., Kong, Q., Zou, W., Parchi, P. & Chen, S. G. Sporadic and familial CJD: classification and characterisation. *Br Med Bull* **66**, 213–239 (2003).

57. Wieser, H. G., Schindler, K. & Zumsteg, D. EEG in Creutzfeldt-Jakob disease. *Clinical Neurophysiology* vol. 117 935–951 Preprint at https://doi.org/10.1016/j.clinph.2005.12.007 (2006).

58. Bishop, M. T., Will, R. G. & Manson, J. C. Defining sporadic Creutzfeldt-Jakob disease strains and their transmission properties. *Proc Natl Acad Sci U S A* **107**, 12005–12010 (2010).

59. Moda, F. *et al.* MM2-thalamic Creutzfeldt-Jakob disease: Neuropathological, biochemical and transmission studies identify a distinctive prion strain. *Brain Pathology* **22**, 662–669 (2012).

60. Meissner, B. *et al. Sporadic Creutzfeldt-Jakob disease Clinical and diagnostic characteristics of the rare VV1 type*. www.neurology.org (2005).

61. Parchi, P. *et al.* Incidence and spectrum of sporadic Creutzfeldt-Jakob disease variants with mixed phenotype and co-occurrence of PrPSc types: An updated classification. *Acta Neuropathol* **118**, 659–671 (2009).

62. Krasnianski, A. *et al.* Clinical findings and diagnostic tests in the MV2 subtype of sporadic CJD. *Brain* **129**, 2288–2296 (2006).

63. Zerr, I. *et al.* Updated clinical diagnostic criteria for sporadic Creutzfeldt-Jakob disease. *Brain* **132**, 2659–2668 (2009).

64. Abu-Rumeileh, S. *et al.* Diagnostic value of surrogate CSF biomarkers for Creutzfeldt-Jakob disease in the era of RT-QuIC. *J Neurol* **266**, 3136–3143 (2019).

65. Hermann, P. & Zerr, I. Rapidly progressive dementias - aetiologies, diagnosis and management. *Nat Rev Neurol* **18**, 363–376 (2022).

66. Wieser, H. G., Schindler, K. & Zumsteg, D. EEG in Creutzfeldt-Jakob disease. *Clin Neurophysiol* **117**, 935–951 (2006).

67. Steinhoff, B. J. *et al.* Diagnostic value of periodic complexes in Creutzfeldt-Jakob disease. *Ann Neurol* **56**, 702–708 (2004).

68. Wieser, H. G., Schindler, K. & Zumsteg, D. EEG in Creutzfeldt-Jakob disease. *Clinical Neurophysiology* **117**, 935–951 (2006).

69. Lee, R. G. & Blair, R. D. G. Evolution of EEG and visual evoked response changes in Jakob-Creutzfeldt disease. *Electroencephalogr Clin Neurophysiol* **35**, 133–142 (1973).

70. Burger, L. J., Rowan, A. J. & Goldensohn, E. S. Creutzfeldt-Jakob disease. An electroencephalographic study. *Arch Neurol* **26**, 428–433 (1972).

71. Neufeld, M. Y. & Korczyn, A. D. Topographic distribution of the periodic discharges in Creutzfeldt-Jakob disease (CJD). *Brain Topography 1992 4:3* **4**, 201–206 (1992).

72. Steinhoff, B. J. *et al.* Diagnostic value of periodic complexes in Creutzfeldt-Jakob disease. *Ann Neurol* **56**, 702–708 (2004).

73. Matsubayashi, T. *et al.* Focal sharp waves are a specific early-stage marker of the MM2-cortical form of sporadic Creutzfeldt-Jakob disease. *Prion* **14**, 207–213 (2020).

74. Zanusso, G. Should MRI signs be included in the diagnostic criteria for sporadic Creutzfeldt-Jakob disease? *Nat Clin Pract Neurol* **2**, 68–69 (2006).

75. Meissner, B. *et al.* MRI lesion profiles in sporadic Creutzfeldt-Jakob disease. *Neurology* **72**, 1994–2001 (2009).

76. Hermann, P. *et al.* Validation and utilization of amended diagnostic criteria in Creutzfeldt-Jakob disease surveillance. *Neurology* **91**, e331–e338 (2018).

77. Rosenbloom, M. H. *et al.* Metabolic disorders with clinical and radiologic features of sporadic Creutzfeldt-Jakob disease. *Neurol Clin Pract* **5**, 108 (2015).

78. Bizzi, A. *et al.* Evaluation of a New Criterion for Detecting Prion Disease With Diffusion Magnetic Resonance Imaging. *JAMA Neurol* **77**, 1141–1149 (2020).

79. McGuire, L. I. *et al.* Real time quaking-induced conversion analysis of cerebrospinal fluid in sporadic Creutzfeldt-Jakob disease. *Ann Neurol* **72**, 278–285 (2012).

80. McGuire, L. I. *et al.* Cerebrospinal fluid real-time quaking-induced conversion is a robust and reliable test for sporadic creutzfeldt-jakob disease: An international study. *Ann Neurol* **80**, 160–165 (2016).

81. Sano, K. *et al.* Early detection of abnormal prion protein in genetic human prion diseases now possible using real-time QUIC assay. *PLoS One* **8**, (2013).

82. Cramm, M. *et al.* Stability and Reproducibility Underscore Utility of RT-QuIC for Diagnosis of Creutzfeldt-Jakob Disease. *Mol Neurobiol* **53**, 1896–1904 (2016).

83. Cramm, M. *et al.* Stability and Reproducibility Underscore Utility of RT-QuIC for Diagnosis of Creutzfeldt-Jakob Disease Abbreviations CI Confidence interval CNS Central nervous system CSF Cerebrospinal fluid diff Difference FFI Fatal familial insomnia PrP C Cellular prion protein PrP Sc Scrapie prion protein PPV Positive predictive value. *Mol Neurobiol* **53**, 1896–1904 (2016).

84. Atarashi, R. *et al.* Simplified ultrasensitive prion detection by recombinant PrP conversion with shaking. *Nat Methods* **5**, 211–212 (2008).

85. Saborio, G. P., Permanne, B. & Soto, C. Sensitive detection of pathological prion protein by cyclic amplification of protein misfolding. *Nature* **411**, 810–813 (2001).

86. Schmitz, M. *et al.* The real-Time quaking-induced conversion assay for detection of human prion disease and study of other protein misfolding diseases. *Nat Protoc* **11**, 2233–2242 (2016).

87. Zerr, I. *et al.* Optimization of the Real-Time Quaking-Induced Conversion Assay for Prion Disease Diagnosis. *Front Bioeng Biotechnol* **8**, (2020).

88. Cramm, M. *et al.* Stability and Reproducibility Underscore Utility of RT-QuIC for Diagnosis of Creutzfeldt-Jakob Disease. *Mol Neurobiol* **53**, 1896–1904 (2016).

89. Zerr, I. Laboratory Diagnosis of Creutzfeldt–Jakob Disease. *New England Journal of Medicine* **386**, 1345–1350 (2022).

90. Telano, L. N. & Baker, S. Physiology, Cerebral Spinal Fluid. *StatPearls* (2022).

91. Spector, R., Robert Snodgrass, S. & Johanson, C. E. A balanced view of the cerebrospinal fluid composition and functions: Focus on adult humans. *Exp Neurol* **273**, 57–68 (2015).

92. Matsumae, M. *et al.* Research into the Physiology of Cerebrospinal Fluid Reaches a New Horizon: Intimate Exchange between Cerebrospinal Fluid and Interstitial Fluid May Contribute to Maintenance of Homeostasis in the Central Nervous System. *Neurol Med Chir (Tokyo)* **56**, 416 (2016).

93. May, C. *et al.* Cerebrospinal fluid production is reduced in healthy aging. *Neurology* **40**, 500–500 (1990).

94. Hrishi, A. P. & Sethuraman, M. Cerebrospinal Fluid (CSF) Analysis and Interpretation in Neurocritical Care for Acute Neurological Conditions. *Indian J Crit Care Med* **23**, S115 (2019).

95. Strimbu, K. & Tavel, J. A. What are Biomarkers? *Curr Opin HIV AIDS* **5**, 463 (2010).

96. Castellani, R. J. *et al.* Sensitivity of 14-3-3 protein test varies in subtypes of sporadic Creutzfeldt-Jakob disease. *Neurology* **63**, 436–442 (2004).

97. Zerr, I. *et al.* Detection of 14-3-3 protein in the cerebrospinal fluid supports the diagnosis of Creutzfeldt-Jakob disease. *Ann Neurol* **43**, 32–40 (1998).

98. Li, Q. X. *et al.* CSF Tau supplements 14-3-3 protein detection for sporadic Creutzfeldt–Jakob disease diagnosis while transitioning to next generation diagnostics. *Journal of Clinical Neuroscience* **50**, 292–293 (2018).

99. van Everbroeck, B., Boons, J. & Cras, P. Cerebrospinal fluid biomarkers in Creutzfeldt-Jakob disease. *Clin Neurol Neurosurg* **107**, 355–360 (2005).

100. Grapp, M. *et al.* Choroid plexus transcytosis and exosome shuttling deliver folate into brain parenchyma. *Nat Commun* **4**, (2013).

101. Kovács, G. G. *et al.* Genetic prion disease: The EUROCJD experience. *Hum Genet* **118**, 166–174 (2005).

102. Uttley, L., Carroll, C., Wong, R., Hilton, D. A. & Stevenson, M. Creutzfeldt-Jakob disease: a systematic review of global incidence, prevalence, infectivity, and incubation. *Lancet Infect Dis* **20**, e2–e10 (2020).

103. Budka', H. *et al. Neuropathological Diagnostic Criteria for Creutzfeldt-Jakob Disease (CJD) and Other Human Spongiform Encephalopathies (Prion Diseases) Neuropathological diagnostic criteria for Creutzfeldt-Jakob disease (CJD) and other human transmissible spongiform encephalopathies (prion diseases) are proposed for t h e following disease entities*. *Brain Pathology* vol. 5.

104. Ghetti, B., Piccardo, P. & Zanusso, G. Dominantly inherited prion protein cerebral amyloidoses - a modern view of Gerstmann-Sträussler-Scheinker. *Handb Clin Neurol* **153**, 243–269 (2018).

105. Adam, M. P., Mirzaa, G. M. & Pagon, R. A. *Genetic Prion Disease*. (2003).

106. Schmitz, M. *et al.* Hereditary Human Prion Diseases: an Update. *Mol Neurobiol* **54**, 4138–4149 (2017).

107. Minikel, E. V. *et al.* Quantifying penetrance in a dominant disease gene using large population control cohorts. *Sci Transl Med* **8**, 322ra9 (2016).

108. Gao, L. P. *et al.* The genetic Creutzfeldt-Jakob disease with E200K mutation: analysis of clinical, genetic and laboratory features of 30 Chinese patients. *Scientific Reports 2019 9:1* **9**, 1–7 (2019).

109. Noble, G. P., Walsh, D. J., Miller, M. B., Jackson, W. S. & Supattapone, S. Requirements for mutant and wild-type prion protein misfolding in vitro. *Biochemistry* **54**, 1180–1187 (2015).

110. Kovács, G. G. *et al.* Genetic prion disease: the EUROCJD experience. *Human Genetics 2005 118:2* **118**, 166–174 (2005).

111. Mitrová, E., Kosorinová, D., Gajdoš, M. & Šebeková, K. A pilot study of a genetic CJD risk factor (E200K) in the general Slovak population. *Tomečková Source: European Journal of Epidemiology* **29**, 595–597 (2014).

112. Kosorinova, D., Belay, G., Zakova, D., Stelzer, M. & Mitrova, E. Genetic risk factors of creutzfeldt-jakob disease in the population of newborns in slovakia. *Pathogens* **10**, (2021).

113. Spudich, S. *et al. Complete Penetrance of Creutzfeldt-Jakob Disease in Libyan Jews Carrying the E200K Mutation in the Prion Protein Gene*. (1995).

114. Bagyinszky, E., van Giau, V., Youn, Y. C., An, S. S. A. & Kim, S. Characterization of mutations in prnp (PRION) gene and their possible roles in neurodegenerative diseases. *Neuropsychiatric Disease and Treatment* vol. 14 2067–2085 Preprint at https://doi.org/10.2147/NDT.S165445 (2018).

115. Ladogana, A. & Kovacs, G. G. Genetic Creutzfeldt–Jakob disease. in *Handbook of Clinical Neurology* vol. 153 219–242 (Elsevier B.V., 2018).

116. Hsiao, K. *et al.* Mutation of the prion protein in Libyan Jews with Creutzfeldt-Jakob disease. *N Engl J Med* **324**, 1091–1097 (1991).

117. Gao, L. P. *et al.* The genetic Creutzfeldt-Jakob disease with E200K mutation: analysis of clinical, genetic and laboratory features of 30 Chinese patients. *Scientific Reports 2019 9:1* **9**, 1–7 (2019).

118. Cohen, O. S. *et al.* Disease duration in E200K familial Creutzfeldt–Jakob disease is correlated with clinical, radiological, and laboratory variables. *J Neural Transm* **126**, 607–611 (2019).

119. Harder*, A. *et al.* Early age of onset in fatal familial insomnia. *J Neurol* **251**, (2004).

120. Chu, M. *et al.* Proposal of new diagnostic criteria for fatal familial insomnia. *J Neurol* (2022) doi:10.1007/s00415-022-11135-6.

121. Chu, M. *et al.* Proposal of new diagnostic criteria for fatal familial insomnia. *J Neurol* (2022) doi:10.1007/s00415-022-11135-6.

122. Chen, C. & Dong, X. P. Epidemiological characteristics of human prion diseases. *Infectious Diseases of Poverty* vol. 5 Preprint at https://doi.org/10.1186/s40249-016-0143-8 (2016).

123. van der Kamp, M. W. & Daggett, V. The consequences of pathogenic mutations to the human prion protein. *Protein Engineering, Design and Selection* vol. 22 461–468 Preprint at https://doi.org/10.1093/protein/gzp039 (2009).

124. Schmitz, M. *et al.* Diagnostic accuracy of cerebrospinal fluid biomarkers in genetic prion diseases. *Brain* **145**, 700–712 (2022).

125. Wu, L. Y. *et al.* Expert Consensus on Clinical Diagnostic Criteria for Fatal Familial Insomnia. *Chin Med J (Engl)* **131**, 1613–1617 (2018).

126. Orrú, C. D. *et al.* Prion Disease Blood Test Using Immunoprecipitation and Improved Quaking-Induced Conversion. *undefined* **2**, (2011).

127. Cramm, M. *et al.* Stability and Reproducibility Underscore Utility of RT-QuIC for Diagnosis of Creutzfeldt-Jakob Disease. *Mol Neurobiol* **53**, 1896 (2016).

128. Schmitz, M. *et al.* The real-time quaking-induced conversion assay for detection of human prion disease and study of other protein misfolding diseases. *Nature Protocols 2016 11:11* **11**, 2233–2242 (2016).

129. Ritchie, D. L. & Ironside, J. W. Neuropathology, immunohistochemistry, and biochemistry in human prion diseases. *Neuromethods* **129**, 79–97 (2017).

130. Zhou, Z. & Xiao, G. Conformational conversion of prion protein in prion diseases. *Acta Biochim Biophys Sin (Shanghai)* **45**, 465–476 (2013).

131. Friedman-Levi, Y. *et al.* PrP ST , a Soluble, Protease Resistant and Truncated PrP Form Features in the Pathogenesis of a Genetic Prion Disease. (2013) doi:10.1371/journal.pone.0069583.

132. Belay, E. D., Blase, J., Sehulster, L. M., Maddox, R. A. & Schonberger, L. B. Management of Neurosurgical Instruments and Patients Exposed to Creutzfeldt-Jakob Disease. *Infect Control Hosp Epidemiol* **34**, 1272 (2013).

133. Mead, S. *et al.* Prion protein monoclonal antibody (PRN100) therapy for Creutzfeldt–Jakob disease: evaluation of a first-in-human treatment programme. *Lancet Neurol* **21**, 342–354 (2022).

134. Minikel, E. V. *et al.* Prion protein lowering is a disease-modifying therapy across prion disease stages, strains and endpoints. *Nucleic Acids Res* **48**, 10615 (2020).

135. Groveman, B. R. *et al.* Extended and direct evaluation of RT-QuIC assays for Creutzfeldt-Jakob disease diagnosis. *Ann Clin Transl Neurol* **4**, 139–144 (2017).

136. Bongianni, M. *et al.* Diagnosis of Human Prion Disease Using Real-Time Quaking-Induced Conversion Testing of Olfactory Mucosa and Cerebrospinal Fluid Samples. *JAMA Neurol* **74**, 155–162 (2017).

137. Orrú, C. D. *et al.* Rapid and Sensitive RT-QuIC Detection of Human Creutzfeldt-Jakob Disease Using Cerebrospinal Fluid. *mBio* **6**, (2015).

138. Foutz, A. *et al.* Diagnostic and Prognostic Value of Human Prion Detection in Cerebrospinal Fluid. *Ann Neurol* **81**, 79 (2017).

139. Franceschini, A. *et al.* High diagnostic value of second generation CSF RT-QuIC across the wide spectrum of CJD prions. *Sci Rep* **7**, (2017).

140. Xiao, K. *et al.* T188K-Familial Creutzfeldt–Jacob Disease, Predominant Among Chinese, has a Reactive Pattern in CSF RT-QuIC Different from D178N-Fatal Familial Insomnia and E200K-Familial CJD. *Neurosci Bull* **35**, 519 (2019).

141. HU, C. *et al.* Cerebrospinal Fluids from Patients with Five Common Genetic Prion Diseases in China Display Distinct Reactivities in the RT-QuIC Assays. *Biomed Environ Sci* **34**, 830–833 (2021).

142. Mok, T. H. *et al.* Bank vole prion protein extends the use of RT-QuIC assays to detect prions in a range of inherited prion diseases. *Sci Rep* **11**, (2021).

143. Sano, K. *et al.* Early Detection of Abnormal Prion Protein in Genetic Human Prion Diseases Now Possible Using Real-Time QUIC Assay. *PLoS One* **8**, (2013).

144. Atarashi, R., Sano, K., Satoh, K. & Nishida, N. Real-time quaking-induced conversion: a highly sensitive assay for prion detection. *Prion* **5**, 150–153 (2011).

145. Lattanzio, F. *et al.* Prion-specific and surrogate CSF biomarkers in Creutzfeldt-Jakob disease: diagnostic accuracy in relation to molecular subtypes and analysis of neuropathological correlates of p-tau and Aβ42 levels. *Acta Neuropathol* **133**, 559–578 (2017).

146. Foutz, A. *et al.* Diagnostic and Prognostic Value of Human Prion Detection in Cerebrospinal Fluid. doi:10.1002/ana.24833.

147. Fiorini, M. *et al.* Molecular Sciences High Diagnostic Accuracy of RT-QuIC Assay in a Prospective Study of Patients with Suspected sCJD. doi:10.3390/ijms21030880.

148. Orrú, C. D. *et al.* Rapid and sensitive RT-QuIC detection of human creutzfeldt-jakob disease using cerebrospinal fluid. *mBio* **6**, (2015).

149. Lattanzio, F. *et al.* Prion-specific and surrogate CSF biomarkers in Creutzfeldt-Jakob disease: diagnostic accuracy in relation to molecular subtypes and analysis of neuropathological correlates of p-tau and Aβ42 levels. *Acta Neuropathol* **133**, 559–578 (2017).

150. Orrú, C. D. *et al.* Rapid and sensitive RT-QuIC detection of human creutzfeldt-jakob disease using cerebrospinal fluid. *mBio* **6**, (2015).

151. Groveman, B. R. *et al.* Extended and direct evaluation of RT-QuIC assays for Creutzfeldt-Jakob disease diagnosis. *Ann Clin Transl Neurol* **4**, 139–144 (2017).

152. Franceschini, A. *et al.* High diagnostic value of second generation CSF RT-QuIC across the wide spectrum of CJD prions. *Scientific Reports 2017 7:1* **7**, 1–8 (2017).

153. Foutz, A. *et al.* Diagnostic and prognostic value of human prion detection in cerebrospinal fluid. *Ann Neurol* **81**, 79–92 (2017).

154. RT-QuIC: a new test for sporadic CJD alison J e Green. doi:10.1136/practneurol-2018-001935.

155. Abu-Rumeileh, S. *et al.* Diagnostic value of surrogate CSF biomarkers for Creutzfeldt–Jakob disease in the era of RT-QuIC. *Journal of Neurology 2019 266:12* **266**, 3136–3143 (2019).

156. Sanchez-Juan, P. *et al.* CSF tests in the differential diagnosis of Creutzfeldt-Jakob disease. *Neurology* **67**, 637–643 (2006).

157. Mattsson, N. CSF biomarkers in neurodegenerative diseases. *Clin Chem Lab Med* **49**, 345–352 (2011).

158. Orrú, C. D. *et al.* A test for Creutzfeldt-Jakob disease using nasal brushings. *N Engl J Med* **371**, 519–529 (2014).

159. Bongianni, M. *et al.* Diagnosis of Human Prion Disease Using Real-Time Quaking-Induced Conversion Testing of Olfactory Mucosa and Cerebrospinal Fluid Samples. *JAMA Neurol* **74**, 155–162 (2017).

160. Kang, X. *et al.* Validation and Application of Skin RT-QuIC to Patients in China with Probable CJD. (2021) doi:10.3390/pathogens10121642.

161. Orrù, C. D. *et al.* Prion Seeds Distribute throughout the Eyes of Sporadic Creutzfeldt-Jakob Disease Patients. *mBio* **9**, e02095-18 (2018).

162. Scott, G., Balsiger, H., Kluckman, M., Fan, J. & Gest, T. Patterns of innervation of the lacrimal gland with clinical application. *Clinical Anatomy* **27**, 1174–1177 (2014).

163. Dartt, D. A. Neural regulation of lacrimal gland secretory processes: Relevance in dry eye diseases. *Prog Retin Eye Res* **28**, 155–177 (2009).

IX. Acknowledgements

I express my sincere gratitude to Prof. Inga Zerr for the opportunity to undertake my Ph.D. study under her supervision, which allowed me to contribute to this great field of prion diseases. I am also extremely grateful to my esteemed supervisor, PD Dr. rer. nat. Matthias Schmitz for his invaluable supervision and treasured support during the course of my Ph.D. degree.

I thank my friends, lab mates, and colleagues, particularly Katrin Tune and Sezgi Canaslan for the support and all the fun moments we had in the last years.

Last but not least, I would like to thank my family: My mother for the unquestionable love and support in my life's greatest and less greatest moments. I am also deeply thankful to her for always believing in and encouraging us to pursue our dreams. I am so grateful to my sister and colleague Angela Silva Correia, for her unquestionable support and contribution to my Ph.D. thesis, for the unlimited hours she spent to help me in the lab, and for the valuable support, she gave me to keep moving forward in my most challenging moments.

X. Supplemental Material

A. Figures

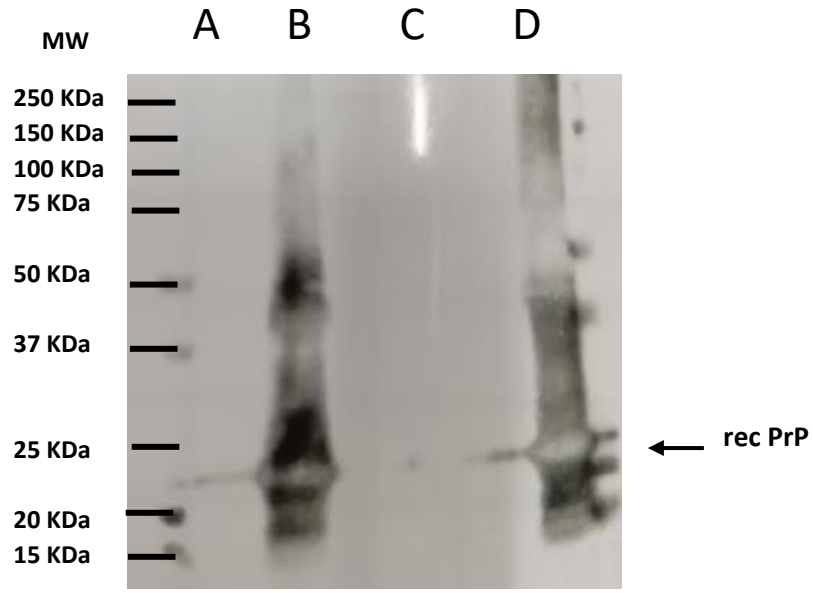

Figure 24. Inclusion bodies purification steps of rec PrP hamster-sheep.

Western blot of inclusion bodies purification steps using Saf 32 antibody (A) Bacteria expression of rec PrP hamster-sheep without adding auto-induction medium. (B) Bacteria expression of rec PrP after overnight with auto-induction medium. (C) Supernatant of the Inclusion bodies centrifugation steps. (D) Inclusion bodies pellet.

A

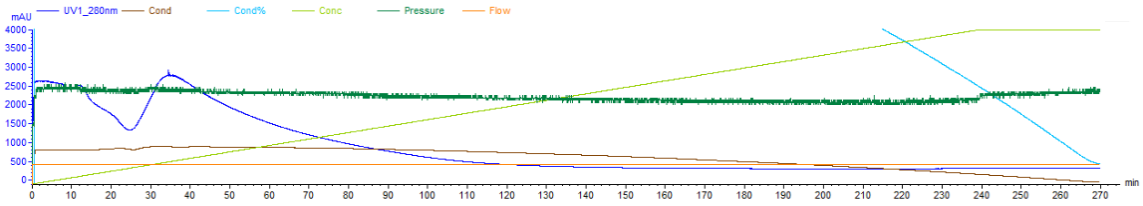

B

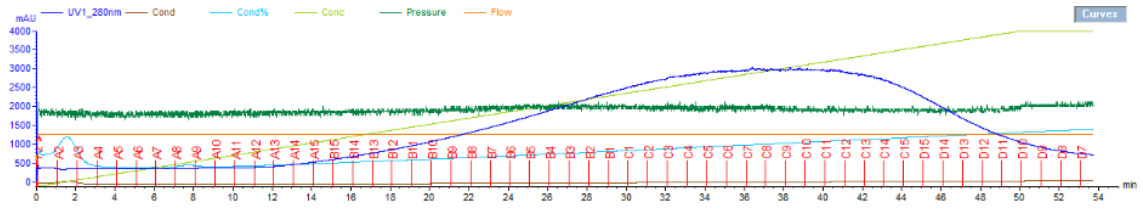

Figure 25. rec PrP hamster-sheep purification using Äkta system.

(A) Refolding step. (B) Elution.

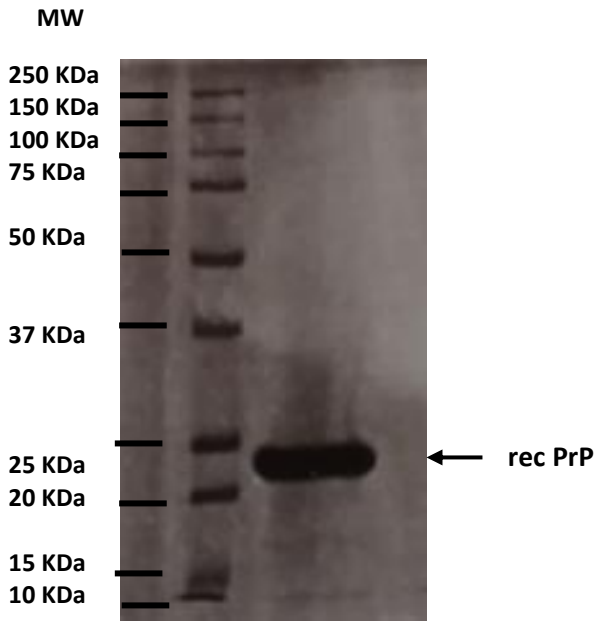

Figure 26. SDS-PAGE of rec PrP hamster-sheep.

Comassie brilliant blue staining of rec PrP hamster-sheep after purification.

Figure 27. Dot blotof rec PrP hamster-sheep after purification using SAF32 antibody

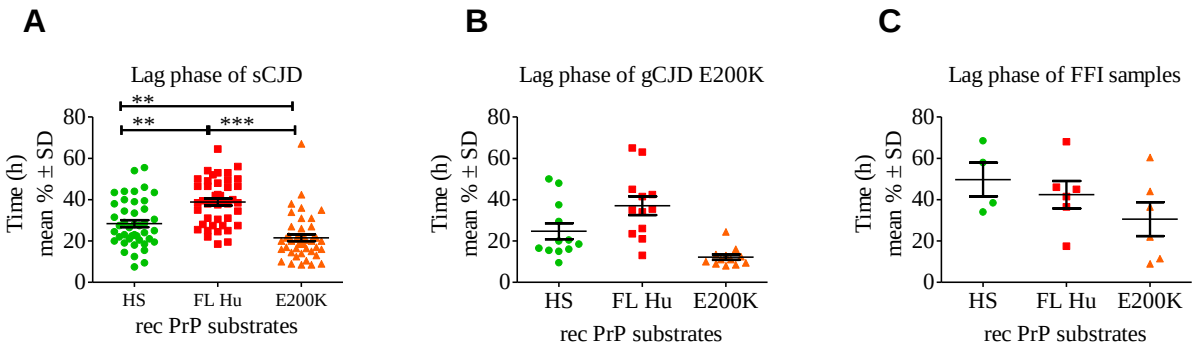

Figure 28. Influence of hamster-sheep, FL Hu, and FL Hu E200K substrates in the RT-QuIC lag phase in sCJD, gCJD E200K and FFI seeded reactions.

RT-QuIC reactions were seeded with CSF from non-CJD controls (n=44) and prion disease patients (n=78 (sCJD), n=17 (gCJD E200K), n=22 (FFI)). Prion disease samples that are positive in all the rec PrP substrates were analyzed.using GraphPad Prism (A) 44 sCJD samples positive in all the rec PrP substrates showed a significant short lag phase when using FL Hu E200K substrate in the RT-QuIC compared to hamster-sheep and FL Hu substrates. (B) RT-QuIC lag phase in 12 gCJD E200K samples positive in all the rec PrP substrates showed no significant difference between substrates. (C) RT-QuIC lag phase in 6 FFI samples positive in rec PrP FL Hu and FL Hu E200K substrates showed no significant difference between substrates.

.